Evaluating Groundwater Exported Acidity in Copano Bay

Final Report

GLO Contract No. 17-180-000-9817

October 14, 2019

Prepared by:
Xinping Hu, Principle Investigator
Dorina Murgulet, Co-Principle Investigator

With assistance from:

Melissa R. McCutcheon, Graduate Research Assistant
Cody V. Lopez, Graduate Research Assistant
Audrey R. Douglas, Graduate Research Assistant

Texas A&M University-Corpus Christi
6300 Ocean Dr., Unit 5860
Corpus Christi, TX 78412
Phone 361-825-3395
Email: Xinping.Hu@tamucc.edu

Submitted to:
Texas General Land Office
1700 Congress Ave.
Austin, TX 78701-1495

A report submitted to the Texas General Land Commissioner pursuant to National Oceanic Atmospheric Administration Award No. is NA16NOS4190174

TABLE OF CONTENTS

ABBREVIATIONS

cm	centimeter
m	meter
km	kilometer
hr	hour
d	day
s	second
$cm \cdot d^{-1}$	centimeter per day
$m \cdot s^{-1}$	meters per second
$m^3 \cdot s^{-1}$	cubic meters per second
$km^3 \cdot d^{-1}$	cubic kilometers per day
$mg \cdot L^{-1}$	milligrams per liter
$\mu g \cdot L^{-1}$	microgram per liter
µL	microliters
mL	milliliter
µM	micromole per liter
$\mu mol \cdot kg^{-1}$	micromoles per kilogram
$\mu mol \cdot d^{-1}$	micromoles per day
SGD	submarine groundwater discharge
^{222}Rn	radon-222
^{223}Ra	radium-223
^{224}Ra	radium-224
^{226}Ra	radium-226
$Bq \cdot m^{-3}$	Becquerels per cubic meter
ERT	electrical resistivity
CRP	continuous resistivity profile Ω-m ohm-meter
TA	total alkalinity
DIC	dissolved inorganic carbon

FIGURE LEGEND

TABLE LEGEND

EXECUTIVE SUMMARY

Copano Bay—the secondary bay of the Mission-Aransas Estuary—has been experiencing long-term symptoms of acidification over the last several decades, including pH and total alkalinity decline, and this has been attributed to decreases in freshwater inflow from rivers. Moreover, there is a clear signature of an additional alkalinity sink in Copano Bay that acerbates the alkalinity decline, particularly during periods of low river discharge hence extended estuarine water residence time. The Mission-Aransas Estuary is the southernmost estuary in Texas that supports a commercial oyster fishery, and oysters are sensitive to changing carbonate chemistry, making it especially important to understand this alkalinity sink and plan appropriately to maintain suitable conditions for healthy oyster growth and production. Based on the changing stoichiometry during drought conditions in a preliminary study, the alkalinity sink cannot be attributed entirely to calcification. The goal of this study was to investigate submarine groundwater discharge as a potential source of acidity driving the alkalinity decline in Copano Bay, and such acid may come from oxidation of reduced species out of sediments via submarine groundwater discharge as observed in other semiarid estuaries.

Two years of monitoring data from Copano Bay show that temporal changes in total alkalinity level are closely tied to river discharge. The influence of submarine groundwater discharge on the solute concentrations of a bay is most notable during periods of low river discharge. While Copano Bay periodically experienced hypersalinity in the past because of low river discharge and high evaporation, such condition was not observed throughout the duration of this project. Regardless, we found notable spatial variability in submarine groundwater discharge based on continuous radon monitoring. Differences in pore water constituents, particularly $\delta^{18}O$

and δD, between years at both transects indicate substantial temporal variability in SGD, likely associated with freshwater inflow differences between years.

Major ion concentrations in the water column all had strong correlation with Cl^- representing conservative mixing. However, pore water major ions including calcium (Ca^{2+}), magnesium (Mg^{2+}), potassium (K^+), and sulfate (SO_4^{2-}) were all measured in excess of the conservative mixing line, indicating that there is production of these ions through SGD and underlying geochemical reactions. The excess sulfate potentially could be a product by oxidation of reduced sulfur products transported into the bay by SGD or pore water recirculation.

Benthic fluxes of alkalinity and DIC show an order of magnitude difference between the values calculated using diffusion and SGD rates, with the latter generating greater fluxes. Diffusion derived DIC flux is ~28% greater than alkalinity flux, although SGD derived alkalinity flux was slightly greater than DIC flux (by ~5%). Oxidation of reduced species from both deeper and shallow pore waters could dampen the net amount of alkalinity flux and lead to a net acidification effect to the estuarine water.

BACKGROUND AND RELEVANCE

Ocean acidification is caused by the invasion of atmospheric CO_2 into ocean surface waters, which has been increasing due to anthropogenic activities including fossil fuel burning, deforestation, and cement production since the beginning of the industrial revolution. Excess CO_2 in the ocean water leads to an increase in proton concentration (i.e., pH decrease) and a decrease in carbonate ion ($[CO_3^{2-}]$) concentration as $[CO_3^{2-}]$ buffers the added acid. A decrease in $[CO_3^{2-}]$ subsequently causes a decrease in carbonate saturation state (Ω) (Feely et al., 2004). Changing carbonate chemistry can negatively affect calcifying organisms by reducing the rates of their shell or skeleton production or making the normal development of juveniles more difficult (Spalding et al., 2017; Waldbusser and Salisbury, 2014). Because numerous calcifying species in the coastal oceans are considered ecosystem engineers or essential members of bottom trophic levels, decrease in calcification is detrimental to the marine environment and can lead to deterioration of ecosystem services that these species provide (Andersson and Gledhill, 2013; Kleypas and Yates, 2009; Waldbusser et al., 2014).

While ocean acidification can be mostly attributed to atmospheric CO_2 increase, carbonate chemistry in estuaries can be influenced by many other factors because of the relatively shallow nature of estuaries and the close proximity of estuaries to terrestrial environments and human activities. Terrestrial input of nutrients and organic matter, tides and mixing, freshwater input, river drainage basin mineralogy, submarine groundwater discharge, and deposition of pollutants (NO_x and SO_x) from ocean vessels (de Weys et al., 2011; Hagens et al., 2014; Hassellöv et al., 2013; Hu and Cai, 2013; Jeffrey et al., 2016; Lin et al., 2004; Ruiz-Halpern et al., 2015) can all affect estuarine carbonate chemistry to various extents. Therefore, estuarine acidification remains a poorly understood problem. However, given that estuaries

provide important ecosystem services and are exposed to potentially increasing number and severity of environmental stressors, it is imperative to examine carbonate chemistry in estuaries in the context of their geomorphology, geographical location, and changing environmental factors.

"Dealkalinzing" estuaries in the northwestern Gulf of Mexico

The lagoonal estuaries of the northwestern Gulf of Mexico coast spread across a climactic gradient, with a freshwater balance (sum of all surface flow and direct precipitation minus evaporation) that is two orders of magnitude greater in the northernmost estuary than the southernmost estuary (Montagna et al., 2013). A recent study based on data collected by Texas Commission on Environmental Quality over the past four decades suggests that the majority of the estuaries in the region have experienced multi-decadal decreases in both alkalinity and pH (Hu et al., 2015). In addition, alkalinity reduction is greater under more saline conditions in estuaries of south Texas, where hypersalinity can develop during prolonged drought (Hu et al., 2015). However, the mechanism for this alkalinity reduction is not entirely clear. Our preliminary data suggest that calcification may account for various degrees of alkalinity reduction in the Mission-Aransas Estuary. In Copano Bay, the secondary bay that connects the Mission and Aransas Rivers and Aransas Bay, up to 85% of alkalinity reduction could not be attributed to calcification (Hu, unpublished data). Therefore, identifying the source of acidity that contributes to such alkalinity consumption is important, especially since oysters are sensitive to this type of change, and the Mission-Aransas Estuary is the southernmost estuary in the state of Texas that supports commercial oyster production (Beseres Pollack et al., 2013).

Submarine groundwater discharge introduced acidity

Groundwater is capable of introducing significant amount of mineral acid to downstream estuaries, a result of oxidation of buried reduced sulfur in coastal wetland environments (Amara et al., 2012; Sammut et al., 1995; Sammut et al., 1996). Typical river water and ocean water mixing would generate a linear relationship between sulfate ion concentration and salinity (or chloride concentration). Hence additional mineral acid production within an estuary would cause a deviation from such relationship, a phenomenon observed in Corpus Christi Bay (Murgulet et al., 2018). Given that estuaries in south Texas mostly experience a shortage of surface inflow (Montagna et al., 2011), relative groundwater discharge would be significant and this may exert some control on the carbonate system, especially in dry years. Therefore, studying the potential effect of groundwater-exported acidity on water carbonate chemistry is important in estuaries that have extensive commercial shellfish production.

Purpose

The extent of submarine groundwater discharge and its role in delivering reduced sulfur to estuaries, which would be oxidized and generate acidity, is unknown in semiarid estuaries. Mineral acid addition into the lagoonal estuaries with long water residence time would play an important role in reducing the total alkalinity inventory, which is potentially detrimental to calcifying organisms and commercial shellfish fisheries. This study examines the effects of groundwater input on alkalinity dynamics and evaluates the pore water-generated sulfide.

This project was designed to achieve the following goals that will improve our understanding of groundwater contribution to water quality degradation in Copano Bay: 1) quantify groundwater discharge and associated export of reduced sulfur at reef and paleovalley margins, 2) quantify the spatio-temporal distribution of reduced sulfur export, 3) examine the

role of groundwater exported reduced sulfur and oyster calcification on the system-wide alkalinity budget. To achieve these goals, we use two approaches: 1) quantify groundwater discharge and reduced sulfur export on a seasonal basis in selected groundwater discharge sites in Copano Bay, and 2) construct a relationship between alkalinity drawdown and acid export using biweekly surveyed surface water data. The product of this project will help resource managers to direct appropriate resources for restoration purposes (such as oyster recycling program) to combat alkalinity loss and to maintain healthy ecosystem functions in environmentally sensitive estuaries such as Copano Bay.

Study Area

This project focused on Copano Bay, the secondary bay of the Mission-Aransas Estuary. Mission-Aransas Estuary was formed from the drowned Mission and Aransas Rivers, has a seafloor composed of terrigenous and biogenic sediments. Copano Bay has several large oyster reefs, three of which are long, straight reefs that run perpendicular to the interior (northwest) shoreline of Copano Bay. Specifically, this study focused on the area crossing the infilled Mission River paleovalley and Copano Reef and continues further into the relict fluvial banks. It also considered the Mission Bay Mouth and adjacent shoreline as reference sampling sites.

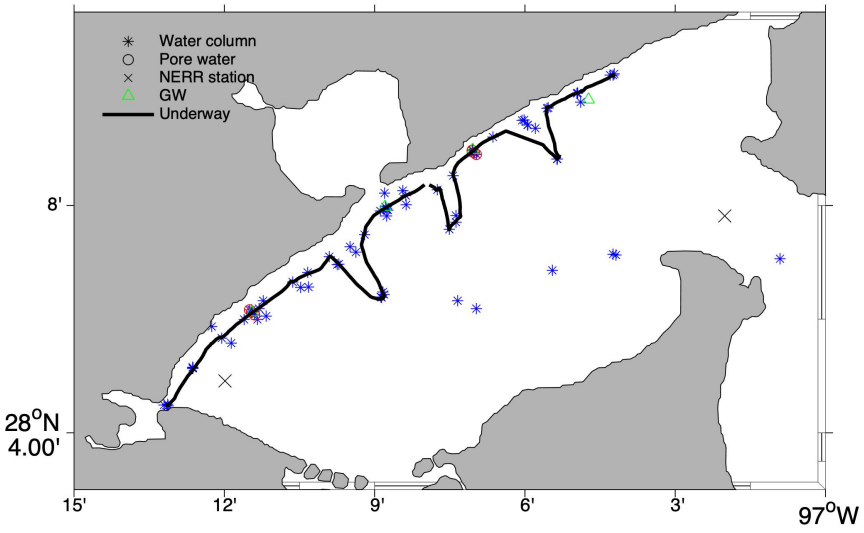

Figure 1 Sampling stations in Copano Bay. The asterisks represent sites where water column samples were collected; the circles represent sites where sediment cores were retrieved and pore water samples were collected. The two crosses represent the two NERR stations (Copano West on the left, and Copano East on the right). The triangles represent stations where deep groundwater samples were collected. The black line represents the underway route along which both radon and CO_2 data were collected.

METHODS

A total of 13 trips (January, 2017 to August 2018) were made to north Copano Bay sampling water column, sediment pore water and underway data (Table 1), one additional trip was made to sample river endmembers on September 1, 2018, and 40 trips were conducted to sample two stations in Copano Bay (Copano West and Copano East, Fig. 1) as a part of the routine national estuarine research reserve survey from September 2016 to December 2018.

Table 1 Sampling information in Copano Bay.

Trip #	Date	Sample type
1	January 21, 2017	Water column, underway, resistivity
2	January 23, 2017	Water column, underway, resistivity
3	July 28, 2017	Water column, underway, continuous radon
4	July 29, 2017	Water column, underway, continuous radon
5	August 9, 2017	Water column, pore water
6	August 11, 2017	Water column, pore water
7	April 27, 2018	Water column
8	June 29, 2018	Water column
9	August 16, 2018	Water column, pore water
10	August 17, 2018	Water column, pore water
11	August 18, 2018	Water column, pore water
12	August 21, 2018	Water column, underway, continuous radon
13	August 22, 2018	Water column, underway, continuous radon
14	Sept 1, 2018	River sampling

Preliminary Investigation

Two day-cruises in January 2017 and two day-cruises in July 2017 were conducted to make a preliminary scan of the entire interior (northwest) shoreline of Copano Bay over two different distinct seasons prior to the site selection for discrete samples and coring. Underway resistivity imaging of the subsurface up to 20 m below the sediment-water interface (using a 112 m graphite electrode cable with 2 m spacing between electrodes) and underway radon monitoring (using a RAD-7 electronic radon detector that measures radon in the air from an equilibrator that received water pumped from the surface of the bay) were conducted during the

day-cruises. Surface water samples for TA, DIC, pH, and major ion concentrations were taken over regular time intervals throughout the underway monitoring.

Sample Collection

Surface and bottom water sample collection

Water samples, used for subsequent chemical and isotope analysis, were collected using a Van Dorn sampler at both the surface and bottom of the water column at each sampling site following the same procedure in Yao and Hu (2017). Unfiltered samples for total alkalinity (TA), pH, and total dissolved inorganic carbon (DIC) analyses were distributed into 250 ml ground neck borosilicate bottles. The samples were preserved with 100 μL saturated mercuric chloride ($HgCl_2$), and the stoppers were sealed using Apiezon® L grease, a rubber band, and a hose clamp. Samples for major ion analysis were filtered through 0.45 μm nylon filters into glass scintillation vials and were later distributed into the appropriate vials for sample dilution or transport. Samples for stable isotope analysis were filtered through 0.45 μm nylon filters into crimp-top vials for analysis. All samples were refrigerated until analysis, and the stable isotope samples were analyzed within two months of collection.

For radiogenic isotope analysis, radon measurements were conducted in the field, as continuous mobile measurements in January and July 2017 and August 2018 along the northern shore of Copano Bay. Samples for radium analysis were collected in three-20L jugs (approximately 45 to 60 L total volume) at each of the spatial sampling sites using a sump pump positioned ~0.2 m above the sediment-water interface.

Pore water sample collection

Pore water was collected in two different manners: large volumes pumped from the sediment and small volumes extracted from intervals within sediment cores. The large volume

pore water samples were collected using a metal piezometer with a retractable tip with screen that was pushed into a permeable layer at ~1 m below the sediment-water interface, off the side of the boat. The piezometer was connected to a peristaltic pump with silicon tubing to suction the pore water out of the sediment. Sample vials were rinsed, filled, and overflowed directly from the tubing extending from the piezometer. Large-volume pore water samples to be analyzed for DIC, TA, pH, major ions, stable isotopes, and radionuclides were all preserved and stored in the same manner as surface water samples.

Small volume pore water samples were extracted using two different methods from sediment cores. Sediment push cores were collected using a home-made corer following the design in Gardner et al. (2009). Cores were pre-drilled at one-centimeter intervals along the length of the core, and holes were temporarily sealed with silicone gel prior to coring. After sampling, the sediment cores were transported to TAMU-CC campus and immediately processed. Water that was overlying the sediment was suctioned from the core at the beginning of the processing to ensure that it did not sink into the core during processing.

The preferred method for extraction of pore water from the cores was using 5 cm, porous, rhizon samplers (Rhizosphere Research Products). The rhizon samplers were inserted into the pre-drilled openings in the core, and pore water was slowly vacuum pulled from the core using a 10 mL, glass, airtight syringe. Pore water was sampled from sediment column depths of around 1, 3, 5, 8, and 12 cm, and samples were pulled sequentially from the shallowest to the deepest interval. The extracted samples were held in the syringes until about 10 mL was extracted, and the sample was then distributed into appropriate sample vials for later analysis.

If pore water sampling via rhizon samplers was not possible (i.e., sediment grain sizes were too small so that sediment particles would clog the rhizon sampler and prevent suction), the

sediment core was cut using a core sectioning device to depth intervals of 0-2, 2-4, 4-6, 6-10, 10-15 cm (representative of the same depth profile that was sampled by the rhizon samplers). The majority of cores were able to be sampled with rhizons for at least the first two intervals, but this method was often required for the deeper intervals in the sediment cores. The sediment slurries were then transferred to plastic closed centrifuge vials and centrifuged at 600 rpm for 10 min to separate pore water from sediment. The supernatant was drawn using a 10 mL syringe and filtered directly into sample vials for TA, DIC, major ion, and stable isotope analysis.

A 4 mL glass, screw-top vial was filled from the bottom for TA and DIC analysis. Due to the small volume, these samples were not preserved with $HgCl_2$. Samples were taped shut and refrigerated until analysis within a month of sample collection. One milliliter of each sample plus 100 µL of concentrated HNO_3 to prevent H_2S from oxidizing to SO_4^{2-} were added to snap-cap vials for Cl-/SO_4^{2-} IC analysis. Two milliliters of sample were collected in a snap cap vial to be used for Ca^{2+} and Mg^{2+} IC analysis. Two different 2 mL crimp-top vials were filled for $\delta^{13}C$ analysis and $\delta^{18}O$ and $\delta^{2}H$ analysis. For H_2S analysis, 1 mL of sample and 0.5 mL $ZnAc_2$ were added to snap-cap vials.

Sample Analyses

Total alkalinity, total dissolved inorganic carbon, and pH analysis

Total alkalinity (TA) was analyzed at 22±0.1°C using Gran titration on an automated titrator (AS-Alk2, Apollo Scitech Inc.). Total dissolved inorganic carbon (DIC) was analyzed using infrared detection on a DIC analyzer (AS-C3, Apollo Scitech Inc.). Certified Reference Material (CRM) was used throughout TA and DIC sample analyses to ensure data quality (Dickson et al., 2003). DIC and TA water column sample analyses had a precision of ±0.1%. The TA and DIC analytical methodology for pore water analyses remained very similar to what we

commonly do (Yao and Hu, 2017) and was only adjusted for smaller volumes. For TA analysis, samples were weighed and pipetted into 4 mL vials of titration samples rather than using the attached Kloehn pump. Lower precision was achieved for pore water samples, with a precision goal of 0.5% for the DIC analyzer. Precision of TA in pore water was uncertain since many samples only had enough volume to be run once.

The pH of water column samples was measured (on total scale) at 25 ˚C using purified m-cresol purple with the spectrophotometric method in Carter et al (2013).

Major ion analysis

Ion chromatography was used to measure major ion concentrations. Pore water samples were diluted to fit the standard range, and the diluted mixtures were pipetted into 2 mL screw cap (with septa), glass vials. Samples for analysis of Cl^- and SO_4^{2-} were analyzed in the lab of co-PI Murgulet using a Dionex High Performance Ion Chromatograph (Model DX600) equipped with an autosampler, an anion-exchange column (7 mm; 4 x 250 mm; Dionex AS14A), and a conductivity detector (Dionex CD25). The detection limit of the method ranged between 0.05 and 0.1 mg/L, depending on the background signal of constituents in the samples.

Undiluted samples for analysis of Ca^{2+} and Mg^{2+} were sealed in 2 mL snap-cap vials and sent to Dr. Alan Shiller's lab at University of Southern Mississippi for analysis.

Stable isotope analysis

Selected water column (estuarine, Mission River) and pore water samples were analyzed for $\delta^{13}C$, $\delta^{18}O$, and δD. Filtered water column and pore water samples for $\delta^{13}C$ analysis were sent to Dr. Jay Brandes' lab at University of Georgia. Filtered water column and pore water samples for $\delta^{18}O$ and $\delta^{2}H$ analysis were done by the Stable Isotope Geoscience Facility (SIGF) at Texas A&M University using a Picarro L2120-I cavity ringdown spectrometer. The isotope ratios are

referenced to the international Vienna Standard Mean Oceanic Water (VSMOW), by way of internal reference standards (JGULF and KONA). Average internal precision is ±0.12‰ for $\delta^{18}O$ and ±0.36 ‰ for δD, and an external precision replicate of the same sample is ±0.26 ‰ for $\delta^{18}O$ and ±1.1 ‰ for δD. $\delta^{13}C_{DIC}$ was determined on a Thermo Fisher Finnigan Delta V isotope ratio mass spectrometer (IRMS) with an Isolink high-performance liquid chromatography (HPLC) preparation module for trace gas samples (Brandes, 2009). Isotopic values were calibrated using chitin standards (Sigma Chemical), which were in turn calibrated to a NIST stable isotope (USGS40) standard. The precision for DIC isotopic composition was ±0.1‰. All stable isotopes are reported using the conventional delta (δ) notation in per mil (‰).

Radiogenic isotope analysis

Radon (^{222}Rn) measurements were conducted continuously along the northern shore of Copano Bay. Water radon concentration was measured continuously using a Durridge RAD7 AQUA accessory connected to a peristaltic pump that extracted bottom water at a rate of approximately 1 L min^{-1}. The gas was continuously circulated within the closed loop and a Durridge Field Drystik, which maintained the humidity under 15%. Air radon concentration was also measured, with an additional Durridge RAD7 unit (Durridge, 2015), to derive bay water degassing flux for the ^{222}Rn mass-balance. Two Durridge RAD7 units were used in the January survey while, during the July 2017 and August 2018 three RAD7 units where used for measurements. In January the count integration time was 15-minute while 10-minute for the other two seasons. Due to setup error, data collected around the North reef on January 23, 2017 were compromised. The northern transect included the survey around the North reef and a return from the Unknown reef, to the South of the North reef.

Radium (radium-223 (^{223}Ra), radium-224 (^{224}Ra), radium-226 (^{226}Ra)) samples were processed by first concentrating the radium onto ~15 g manganese dioxide (MnO_2) impregnated acrylic fibers by passing the sample through the fibers two times at a flow rate <1 $L \cdot min^{-1}$ (Dimova et al., 2007; Kim et al., 2001). The Mn-fibers were then rinsed thoroughly with Ra-free water to eliminate any salts or particulates and then pressed to a water to fiber ratio of 0.3-1 g (i.e., 20-30 g wet weight) (Sun and Torgersen, 1998). The fibers were tested for the short-lived ^{223}Ra (half-life: 11.4 days) and ^{224}Ra (half-life: 3.6 days) on a Radium Delayed Coincidence Counter (RaDeCC). Activities of ^{224}Ra were measured within three days of collection given the short half-life (Moore, 2006). After the short-lived isotope measurements, the fibers were flushed with nitrogen gas and sealed for >21 days to reach secular equilibrium before ^{226}Ra (half-life: 1,600 years) activity is measured on a RAD-7 with measurements corrected to a calibration curve determined from 5 standards (Moore, 1996). Only the large-volume pore water samples underwent radiogenic isotope analysis (not the pore water extracted from cores). Measurements of radon (^{222}Rn) 250 mL grab samples (pore water) were conducted using a Durridge RAD7 radon-in-air monitor with the soda bottle and WAT250 accessories and protocols, respectively (Lee and Kim, 2006). The accessories are used to sparge the gas from the water bringing it into a closed air loop and to the detector.

Submarine Groundwater Discharge Estimates

SGD rates were calculated from continuous ^{222}Rn and Ra activities, as described below.

Radium Ages

Relative radium age of the surface water, or the relative time that has passed since the radium first entered the system in a well-mixed estuary, was calculated using the ratio of the

short-lived (^{224}Ra) to the long-lived (^{223,226}Ra) isotopes using Equation 1 from (Knee et al., 2011):

$$T_w = \frac{AR_{GW} - AR_{CO}}{AR_{CO} \times \lambda_{224}} \quad (1)$$

where AR_{GW} is the initial activity ratio of discharging groundwater, AR_{CO} is the measured activity ratio at the station of interest, and λ_{224} is the decay constant (d^{-1}) for the short-lived radium-224 isotope (Knee et al., 2011). This equation assumes radium activities and activity radios are greatest in the Ra source (i.e. groundwater and sediment containing Ra) and also elevated in receiving nearshore water relative to waters further offshore due to SGD and desorption from sediments. Consequently, radium activities and ARs should be decreasing as the water mass is moving away from the discharge point. This could occur due to two factors: radioactive decay and mixing with more dilute offshore waters. This equation also assumes Ra additions are occurring continuously over a wide area, in this case the northern Copano Bay with multiple groundwater discharge locations. The short-lived isotope is normalized to the long-lived isotope (i.e. ^{226}Ra) with activities that are expected to only decrease due to dilution. Because the half-life of ^{226}Ra is much longer ($T_{1/2}$ = 1600 yr) with respect to mixing time, its decay rate is negligible. Using the groundwater activity ratios as the source of radium (i.e. water source), an estimate of the time since SGD occurred was provided.

It should be noted that water mass ages and residence times are different ways to quantify mixing within a water body and they may not yield the same results since residence times calculate the amount of time it takes a parcel of water to leave the water body whereas water mass ages calculate the length of time since a parcel of water entered the water body.

Radium-derived SGD estimates

To estimate SGD from Ra observations in Copano Bay, an estuarine mass balance is required to determine the excess inventory of Ra (i.e., due to groundwater flux) in the bay. This mass balance includes all sources of Ra other than groundwater such as: tidal exchange, rivers, desorption from riverine suspended sediments, diffusion from sediments (Moore, 1996). Expressed mathematically, excess Ra (Ra_{ex} [$Bq \cdot d^{-1}$]) in the bay equals:

$$^{226}Ra_{ex} = \left(\frac{(^{226}Ra_{CB} - ^{226}Ra_{OS}) \times V_{CB}}{T_w}\right) - \left(^{226}Ra_R \times Q_R\right) - \left(^{226}Ra_{des} \times TSS \times Q_R\right) \quad (2)$$

where Ra_{CB} is the average measured activity in Copano Bay, Ra_{OS} is the average activity in the offshore water body (i.e. mid-bay) which exchanges tidally, V_{CB} is the volume of Copano Bay, T_w is the residence time estimated from the apparent radium water ages, Q_R is the average total discharge rate of the tributaries to the bay, Ra_R is the average activity of the tributaries, and Ra_{des} is the activity of the radium desorbed by the sediments in the bay (Charette et al., 2001a; Swarzenski, 2007). After accounting for all possible sources of Ra, it is assumed that the excess activity from equation (2) is the result of SGD. Thus, using a groundwater (i.e., porewater) endmember activity (Ra_{PW}), SGD is calculated from:

$$SGD = \frac{^{226}Ra_{ex}}{^{226}Ra_{GW}} \quad (3)$$

Radium desorption experiments were conducted using representative riverine sediment samples (i.e., 0-10 cm) from the freshwater portion of Aransas and Mission rivers following the methods outlined by Douglas et al. (in review). Bay and River water samples were filtered through Whatman GF/F filters to remove suspended solids and then processed through MnO_2 fibers to remove any radium. Solutions of Ra-free river and bay water were made to match salinities at the time of sample collection (2017: August 9-11, 2018: August 17-18). A known mass of dried sediments was added to a known volume of the Ra-free solutions in proportions mimicking naturally occurring total suspended solids (TSS) expected for the study area. Sample

solutions were then slurried and placed on a shaker table for 45 minutes before extracting the desorbed radium by passing the solution through MnO_2 fibers and processing as described above. Total Ra activity was normalized to the sediment mass and then multiplied by the sediment flux from the rivers (Lopez et al., 2018).

Radon-derived SGD estimates

Radon is much more enriched in groundwater when compared to surface waters (typically 1000-fold or greater) (Dimova et al., 2011). Because of its unreactive nature and short half-life ($T_{1/2}$ = 3.83 d), ^{222}Rn is an excellent tracer to identify areas of significant groundwater discharge (Burnett and Dulaiova, 2003). Recent studies demonstrated that continuous radon measurements could provide reasonably high-resolution data to evaluate changes of radon concentration of surface water at one location over time (Burnett and Dulaiova, 2003; Burnett et al., 2001). Continuous (in-situ or mobile) measurements of ^{222}Rn were conducted over two days along the northern Copano bay in both July 2017 (Spalt et al., 2018) and July 2018 with three RAD-7s connected in parallel and the RAD AQUA accessory. During mobile continuous measurements of ^{222}Rn, the use of multiple detectors connected in line yielded a 10-min integration time (or an integrated measurement every ~0.7 km), which provided increased spatial resolution, thus better precision in locating spatial heterogeneity of SGD. The monitoring system measured ^{222}Rn from a constant stream of water (driven by a peristaltic pump) passing through an air-water exchanger. The exchanger distributed radon from a running flow of water to a closed air loop that feeds to the RAD-7 detectors. The continuous ^{222}Rn measurements were compiled and used to construct a mass balance to estimate SGD as described in detail in Spalt et al. (2018), and references therein. Expressed mathematically, the total ^{222}Rn flux (F_{total}) equals:

$$F_{total} = [z(\lambda A_{Rn} - \lambda A_{Ra})] - F_{sed} + F_{atm} \pm F_{mix}$$

where λA_{Rn} is the decay corrected activity of ^{222}Rn in water column, λA_{Ra} is the activity of ^{222}Rn due to production ^{226}Ra in the water column, z is the water depth, F_{sed} is the sediment flux, F_{atm} is the losses due to atmospheric evasion, and F_{mix} is the losses due to mixing processes. Thus, changes over time, if any, may be converted to radon fluxes. Using the advective fluid radon activities, ^{222}Rn fluxes were converted to water fluxes (Burnett and Dulaiova, 2003):

$$w\ (m \cdot s^{-1})\ = \frac{F_{total}}{^{222}Rn_{GW}}$$

Tidal effects could not be fully addressed using the presented methods; however, given the microtidal characteristics of this system, tidal effects are expected to be minimal compared to wind-driven circulation (Santos et al., 2012). Nevertheless, changes in water levels of no more than 0.3 m are recorded in this area due to tidal fluctuations (NOAA 2014). It is assumed that the lower radon fluxes observed during the monitoring time are due to mixing with offshore waters of lower activity. The maximum absolute values of the observed negative fluxes during each time-series event at each location were used to correct radon fluxes for losses via mixing (Burnett and Dulaiova, 2003; Dulaiova et al., 2006). Sediment-supported radon activities were measured using laboratory equilibration experiments from sediment cores collected from each box following the methods outlined by Corbett et al. (1998). ^{226}Ra samples (18-40 L) collected in each box were used to correct for in-situ production of ^{222}Rn. Wind speed data were obtained from the National Data Buoy Center using buoy MAXT2 from the National Estuarine Research Reserve System.

RESULTS AND DISCUSSION

Preliminary Investigation

Two 2-day trips were carried out in January and July, 2017 to measure surface water radon activity, salinity, CO_2 fraction (xCO_2) and pH using underway approaches. General observation revealed that the transect close to the Aransas River mouth (lower left corner) generally had lower salinity and xCO_2, higher pH and radon activity (Fig. 2 and 3). Note the January 23 survey likely had erroneously high xCO_2 readings because setup error (Fig. 2), which has also affected the radon measurements. The river influence on estuarine carbonate chemistry is likely a result of riverine enhanced surface primary production during our surveyed times, which consumes CO_2, elevated pH. In the July 2017 surveys, surface water near the oyster reefs appeared to have higher levels of xCO_2 and lower pH (Fig. 3). Interpretation of electrical resistivity surveys conducted during the 2017 January trip are included in the Spalt et al. (2018) paper.

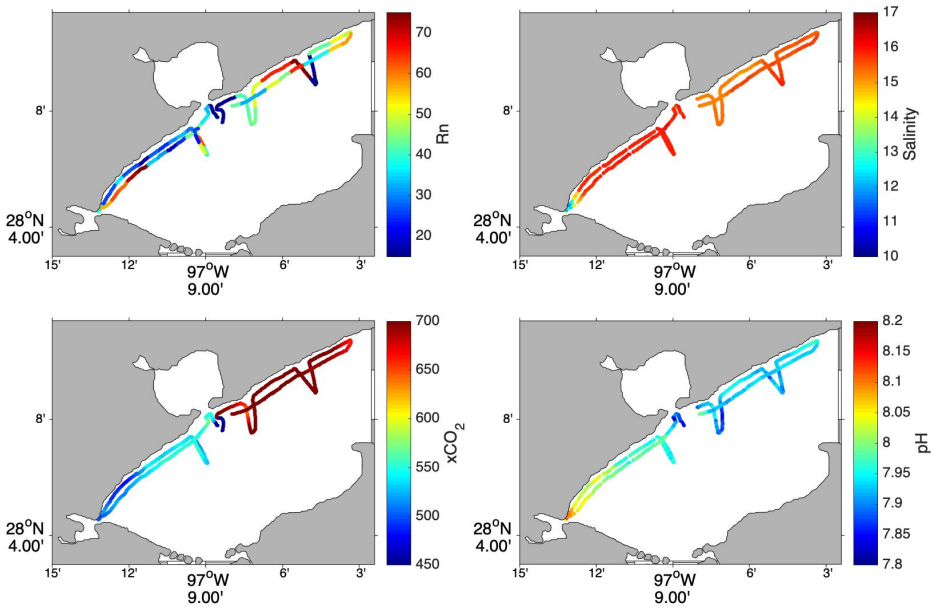

Figure 2 Spatial survey of radon, salinity, CO_2 fraction (xCO_2), and pH (January 21 and 23, 2017).

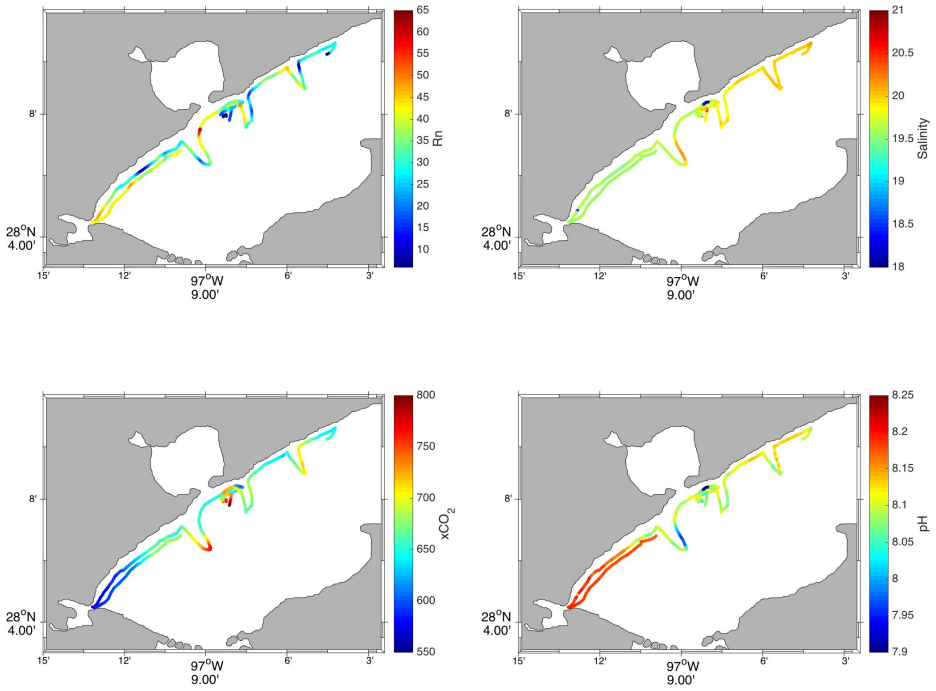

Figure 3 Spatial survey of radon, salinity, CO_2 fraction (xCO_2), and pH (July 28-29, 2017).

Spatial and Temporal Data Assessment

Radium activities and SGD rates

Activities of ^{226}Ra were in average 850.9±8.5 dpm·m^{-3} (n=12) across all seasons. The highest average ^{226}Ra surface water activity was measured in July 2017 ($\bar{x}$: 975±9.8 dpm·m^{-3}; n=6), while the lowest occurred in August ($\bar{x}$: 853.3±8.5 Bq·m^{-3}; n=6)**.** The highest activity in July 2017 was measured to the south of Mission Bay while in August 2018, the highest ^{226}Ra was found to the north (Fig. 4**)**. The lowest activities overall occur in August, the season with the lowest salinities, potentially as a result of mixing with depleted, fresh riverine waters. Activities of ^{2244}Ra were in average 956.9±9.6 dpm·m^{-3} (n=12) across all seasons. The highest average ^{224}Ra surface water activity was measured in July 2017 ($\bar{x}$: 1,022.7±10.2 dpm·m^{-3}; n=6), while the lowest occurred in August ($\bar{x}$: 725.7±7.3 Bq·m^{-3}; n=6)**.** The highest activities in July and August were measured at the same locations as with ^{226}Ra (Fig. 4).

Activities of ^{223}Ra were on average 75.8±0.8 dpm·m^{-3} (n=12) across all seasons. The highest average ^{223}Ra surface water activity was measured in July 2017 ($\bar{x}$: 87.9±0.9 dpm·m^{-3}; n=6), while the lowest occurred in August 2018 ($\bar{x}$: 62.5±0.6 Bq·m^{-3}; n=6)**.** The lowest activities overall for all three isotopes occurred in August 2018, the season with the lowest salinities, potentially as a result of mixing with depleted, fresh riverine waters. Although not strong, some slight positive relationships exist between salinity and ^{223}Ra, ^{224}Ra and ^{226}Ra (R^2: 0.2; 0.58; and 0.36, respectively). Desorption of radium from sediments is expected to increase with increasing salinity (Elsinger and Moore, 1980; Webster et al., 1995). With fresh riverine inputs, a decrease in the radium activities is expected, thus a positive relationship as observed here.

Like surface water, average porewater activities of ^{226}Ra are larger in July 2017 ($\bar{x}$: 1531.5±15.3 dpm·m^{-3}; n=4) compared to August 2018 ($\bar{x}$: 1158.4±11.6 dpm·m^{-3}, respectively;

n=4). On the other hand, ^{223}Ra and ^{224}Ra actives were higher in August 2018 ($\overline{x}$: 222.8±2.2 and 4901.6±49 dpm·m^{-3}, respectively in July 2017 versus 269.6±2.7 and 5132.6±51 dpm·m^{-3}, in August 2018, respectively). On average, higher salinity was observed in July ($\overline{x}$: 20) when compared to August ($\overline{x}$: 15) but no statistical correlation was found between salinity and radium (R^2~0.01). This could indicate that changes in radium between the two seasons are not the result of salinity changes, especially since larger short-lived isotope activities are measured at the lower salinity end. Although it could be argued that the short-lived isotopes (radium-224 and radium-223) recovery is much faster than the long-lived radium-226 which will be found in lower activities at the lower salinity end. Nevertheless, the increase in the short-lived isotopes from the more saline season to the fresher one, suggests that additional input from groundwater is likely occurring.

Radium desorption from sediments is expected to reach a maximum at an approximately salinity of 20 (Elsinger and Moore, 1980; Webster et al., 1995) thus a positive relationship is expected given changing salinities. Thus, these observed increases in the short-lived isotope activities following a wet period and the expected recharge of water table and increased hydraulic gradients towards to bay likely explain input of young terrestrial waters through lateral subsurface transport. The long-lived isotope ^{226}Ra is, thus, diluted with younger groundwaters that are expected to be more depleted in this isotope in the shallow groundwater as indicated by Spalt et al. (2018). The input of young, fresher groundwaters in August 2018 is also supported by the more depleted δ^{18}O and δD isotope signatures in the porewater and the positive correlation between salinity and the δ^{18}O and δD (R^2: 0.89 and 0.86, respectively).

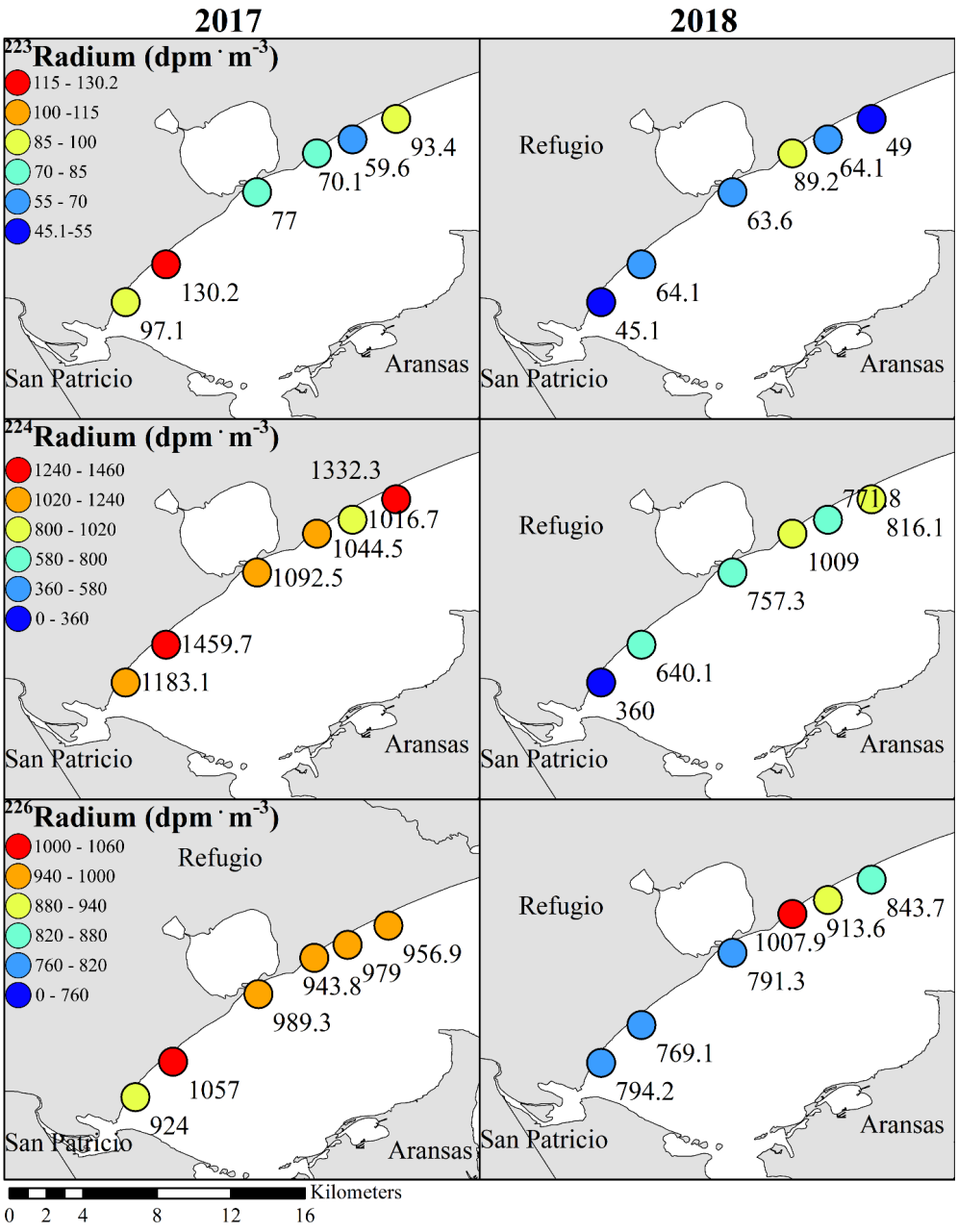

Figure 4 Activities of radioisotopes from samples collected during August 9-12, 2017 and August 17-18, 2018.

Radium SGD discharge rates

Radium-derived SGD rates, representative of the saline component of total SGD, are slightly larger in July 2017. Using the seasonal porewater ^{226}Ra endmembers and corresponding surface water radium ages derived using the rasium-224/radium-223 activity ratios, SGD rates are

estimated to be 10.8±1.08 cm·d^{-1} for July 2017, and 7.24±0.7 cm·d^{-1} for August 2018. When the porewater ^{223}Ra endmember and the associated surface water radium ages (also derived using the rasium-224/radium-223 activity ratios are used), SGD rates were 9.31±0.9 cm·d^{-1} for July 2017, and 5.12±0.51 cm·d^{-1} for August 2018. These slightly lower estimates, compared to those using ^{226}Ra, are likely the result of salinity effects on radium and, thus, signify a lower input of saline SGD during a wet season.

The slight seasonal variability is directly related to changes in the porewater and surface water activities as they influence the water ages, the ^{226}Ra inventory, and the conversion to a final bay wide SGD (Charette et al., 2001b). For instance, ^{226}Ra decreased in surface water and pore water from July 2017 to August 2018. However, ^{224}Ra and ^{223}Ra decreased in surface water but increased in porewater from July 2017 to August 2018 (Table 2). In addition, differences in the two radium isotope estimates result from their different inputs and response to salinity effects (sorption with decreasing salinities and desorption with increasing salinity). Nevertheless, the two methods agree very well for both seasons and closely match the ^{222}Rn-derived estimates (Table 2), which are only twice as high in July 2017 and about four times greater in August 2018.

Table 2 Radium and radon-derived bay-wide SGD rates for the July 2017 and August 2018 sampling events. End-members chosen derive the radon-based SGD were 8693 Bq·m^{-3} for the upper limit, 10840 Bq·m^{-3} for the average, and 14509 Bq·m^{-3} for the lower limit. The radon end-members were derived from groundwater wells in the Copano watershed, the highest observed porewater activity, and the highest observed groundwater well activity for the upper, average, and lower limit respectively (Spalt et al., 2018). (unit: cm d^{-1})

2017			2018		
Ra-223	Ra-226	Rn-222	Ra-223	Ra-226	Rn-222
9.31±0.93	10.8±1.08	Upper Limit: 29.6±1.42 Average: 23.8±1.14 Lower Limit: 17.7±0.85	5.12±0.51	7.24±0.7	Upper Limit: 26.0±2.48 Average: 20.9±1.99 Lower Limit: 15.6±1.49

Radon activities and SGD rates

Continuous measurements of ^{222}Rn activities were measured during the January and July 2017 and August 2018. The 2017 surveys are generally higher in radon proximity to the reefs and to the south of Mission Bay (Figure 5; Table 3). SGD rates derived from ^{222}Rn activities for January and July 2017 are already described in Spalt et al. (2018). Similar to this study, to account for the possible uncertainties related to the groundwater endmember, for SGD estimates the following groundwater endmembers were used: the highest and average groundwater (14,508 and 8,693 Bq m^{-2}, respectively) and highest porewater (10,840 Bq m^{-2}) ^{222}Rn activities.

Briefly, the largest ^{222}Rn activities (both min and max) were measured in January 2017 along the northern transect but also on the further offshore transect in the southern transect (Table 3; Figure 5). Both July 2017 and August 2018 show lower ^{222}Rn activities. Overall SGD rates are greater in January in both southern and northern transect (Table 3).

Table 3 Minimum, maximum and average radon measured in water during the three mobile radon surveys in Bq·m-3. SGD for the Upper, Middle, and Lower range end-members are also presented, in cm·d-1, for both the Northern and Southern transects as well as overall average.

	Location	Northern Transect			Southern Transect			North and South Transect		
	Event	Jan-17	Jul-17	Aug-18	Jan-17	Jul-17	Aug-18	Jan-17	Jul-17	Aug-18
Rn	Min.	31.9 ±3.2	6.5 ±0.7	14.1 ±1.4	16.4 ±1.6	6.3 ±0.6	8.8 ±0.9	16.4 ±1.6	6.3 ±0.6	8.8 ±0.9
	Max.	75.2 ±7.5	52.1 ±5.2	57.6 ±5.8	74.9 ±7.5	62.1 ±6.2	55.2 ±5.5	75.2 ±7.5	62.1 ±6.2	57.6 ±5.8
	$\bar{x}$	48.1 ±4.8	31.7 ±3.2	35.6 ±3.6	37.9 ±3.8	35.6 ±3.6	23.7 ±2.4	41.9 ±4.2	34.0 ±3.4	29.9 ±3.0
	n	19	30	30	30	43	28	49	73	58
SGD	Uppr.	62.7 ±5.5	29.0 ±2.7	31.7 ±3.6	48.2 ±4.9	30.1 ±1.5	19.2 ±3.0	54.0 ±3.8	29.6 ±1.4	26.0 ±2.5
	Mid.	50.3 ±4.4	23.2 ±2.2	25.4 ±2.9	38.7 ±3.9	24.1 ±1.2	16 ±2.4	43.3 ±3.0	23.8 ±1.1	20.9 ±2.0
	Low	38.2 ±3.2	17.4 ±1.6	19 ±2.1	28.5 ±2.9	18.0 ±0.9	11.9 ±1.8	32.3 ±2.3	17.7 ±.9	15.6 ±1.5
	n	19	30	30	30	43	28	49	73	58

The largest seasonal differences are observed for the northern transect where the July 2017 and August 2018 rates are lower by approximately 50% than in January 2017 (Figure 5, Table 3).

SGD rates in the southern transect also decrease between January and July 2017, but to a lower extent. This is, however, related to wind effects as explained by Spalt et al. (2018). Large temporal variation in wind speed between the three surveys (January: max. 38.4, min. 15.1, $\bar{x}$ 22.6; July: max. 29.4, min. 2.3, $\bar{x}$ 17.5; August: max. 15.5, min. 6.7, $\bar{x}$ 9.4 wind speed in $km \cdot h^{-1}$) could potentially lead to significant ^{222}Rn degassing, thus lower calculated SGD rates. Losses that are unaccounted for in the inventories and SGD calculations are expected and should be further investigated (Williams and Follows, 2011). A decrease of more than 50% in SGD rates was also observed for the southern transect from January 2017 to August 2018. The August 2018 survey occurred following a wet period with significant surface runoff inputs (Figure 6). Thus, the overall role of SGD in the bay's water budget may be lower during the wet periods, although January 2017 was also slightly wetter than July 2017 (Figure 6).

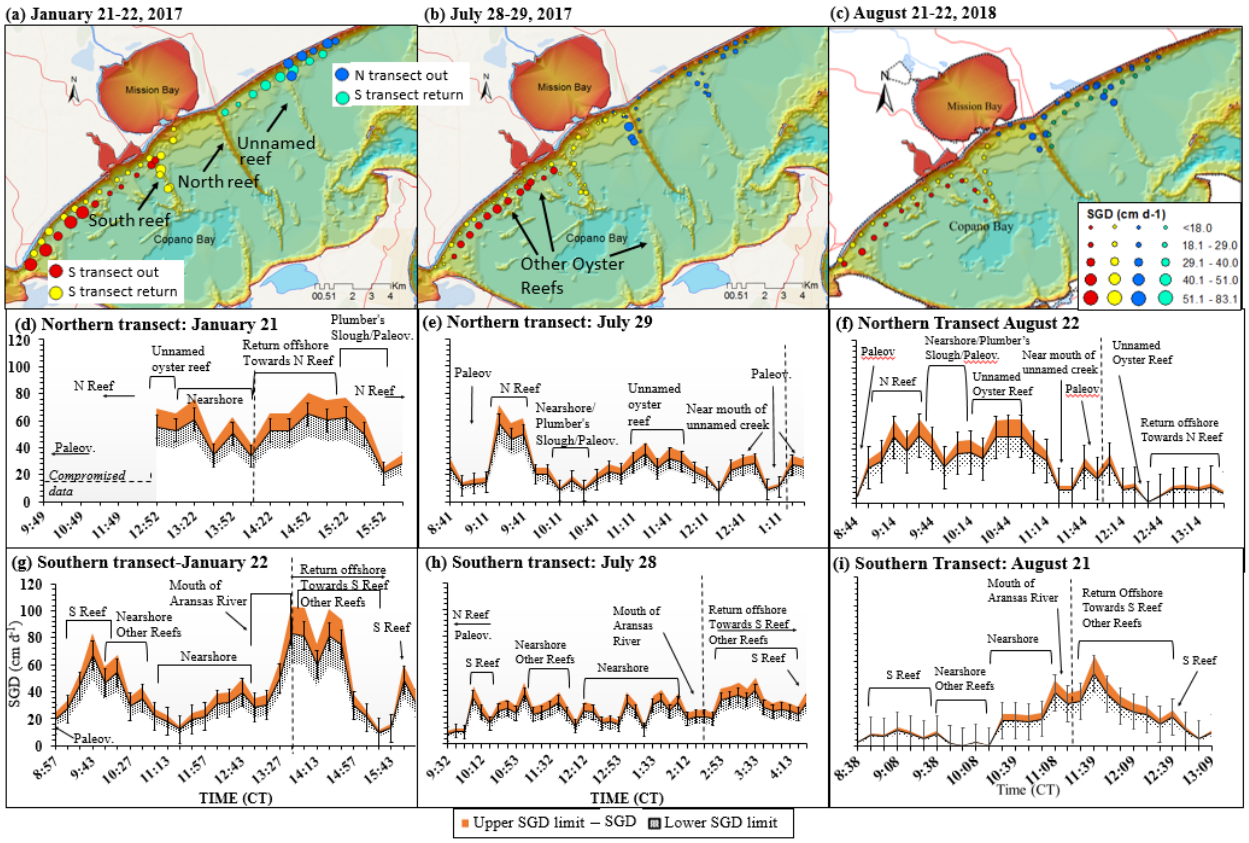

Figure 5 Continuous SGD surveys for January (a) and (b), 2017 and August 2018. The background in the top maps (a and b) is bathymetry (NOAA, 2016) showing the higher seafloor

elevation at the main reefs (see Spalt et al., 2018) and other smaller unnamed reefs which are pervasive within Copano Bay and in proximity to the North shoreline. Spatial magnitude of SGD (a-c) is depicted using filled circles of different sizes and colors. Magnitudes of SGD rates with time are depicted for the surveys going out and return to the Mission Bay mouth along the southern (d, e, f) and northern (g, h, i) and shores.

SGD rates method intercomparison

In this study, we observed differences between the radon and radium SGD estimates similar to those in Baffin Bay (Lopez et al., 2018). Radium estimates were only conducted for the July 2017 and August 2018 surveys. These events captured differences in hydroclimatic conditions (Figure 6) which resulted in more variable radium activities in the subsurface estuary/groundwater and surface water due to salinity effects (Cerdà-Domènech et al., 2017). While radon is unreactive and produces estimates of total SGD (including fresh and saline terrestrial groundwater and recirculating seawater) (Burnett and Dulaiova, 2003), salinity-dependent radium may only provide the saline portion of SGD and misses its fresher component (Moore, 2006). It is expected that during groundwater upwelling, radium is sequestered into sediment particles, which leads to lower surface water inputs. However, since radon-derived rates (or total SGD) are similar among the two seasons (July 2017 and August 2018), lower radium rates are indicative of reduced saline inputs during wet periods. In this study, the saline SGD component is up to one half of the total SGD during a dry season (e.g., July 2017) and up to a fourth during a wet season (e.g., August 2018).

Hydrographical changes in Copano Bay

Significant changes in river inflow occurred during the project period as indicated in the amount of river discharge (Fig. 6a). From the inception of this project (September, 2016) till late August, 2017, there was minimal precipitation and river discharge. As a result, estuarine salinity exhibited a monotonic increase (Fig. 6b). In the end of August, 2017, significant river discharge occurred, which was followed by large decrease in salinity in Copano Bay. Between this river

discharge event and the next one in mid-June, 2018, salinity increased again (Fig. 6b). The rest of the sampling period was punctuated by more frequent river discharge hence salinity remained at relatively low levels.

Similar to salinity variation, total alkalinity also exhibited similar pattern, although the increase tended to level off during the prolonged drought conditions. The localized sampling in north Copano Bay revealed broad agreement with data from the two NERR sites (Fig. 7).

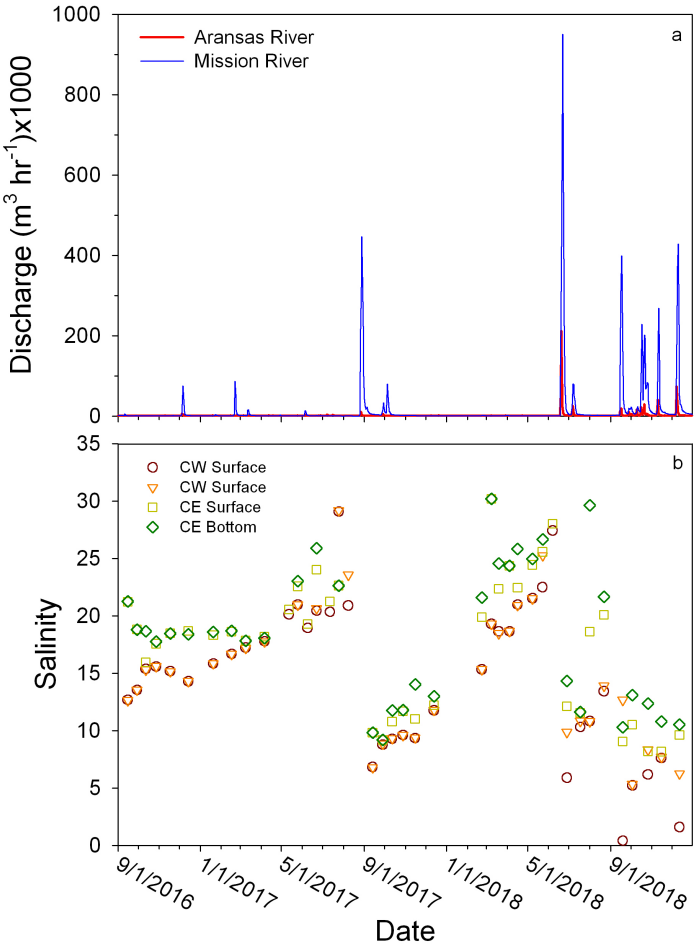

Figure 6 (a) Discharge from Aransas (red) and Mission (blue) rivers; (b) Surface and bottom water salinity at Copano West (CW) and Copano East (CE) stations.

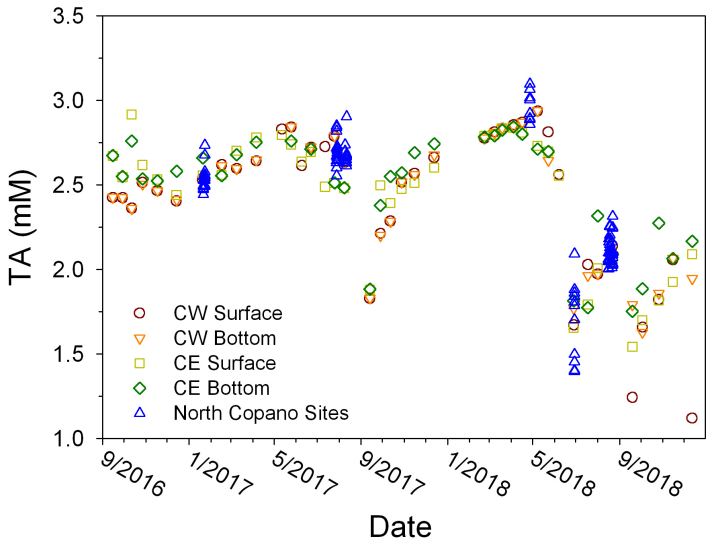

Figure 7 Temporal changes in total alkalinity in Copano West (CW) and Copano East (CE) stations. The triangles represent data from the north Copany Bay sites during all field surveys for pore water and underway measurements.

Major Ion Chemistry in Water Column

All major ions (Ca^{2+}, Mg^{2+}, K^{+}, SO_4^{2-} and Br^{-}) exhibited excellent linear relationship with Cl^{-} (Table 3), the dominant anion in the water column and indicator for seawater dilution by river water (Fig. 8). This relationship is expected as river water contains minimal levels of ions. However, in some of the samples collected from the overlying waters of sediment cores (August 11, 2017, Table 1), SO_4^{2-} exhibited excess relative to Cl^{-} (light green squares in Fig. 8a), while none of the other major ions had excess signal, indicating that sulfate was released into the overlying water, likely due to disturbance to the sediment-water interface during the transit from the field to the TAMU-CC lab.

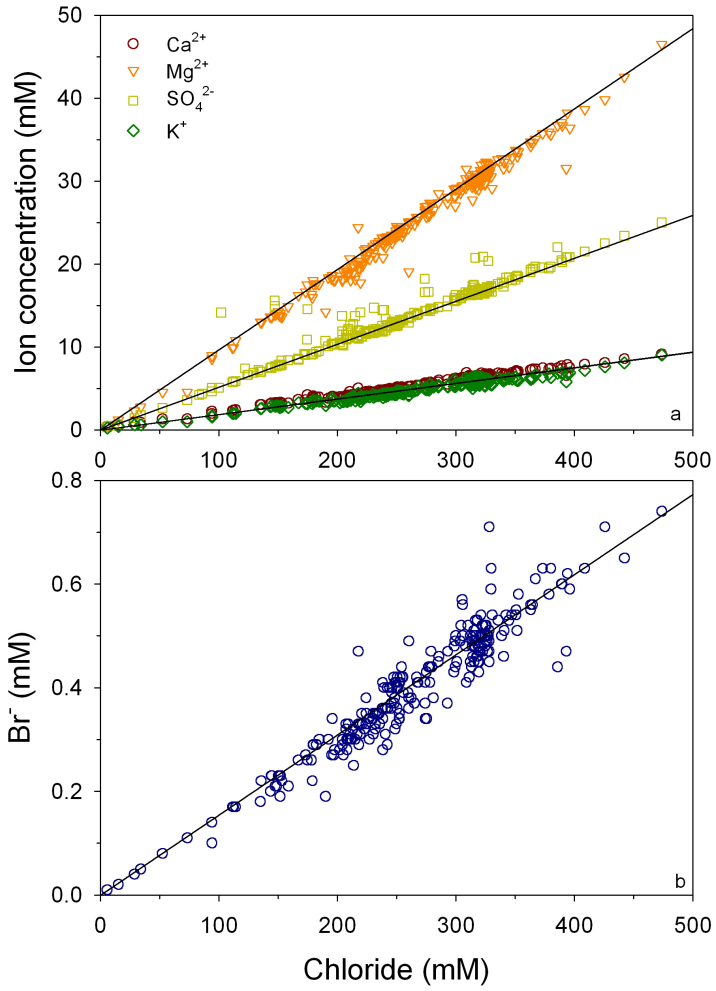

Figure 8 Correlation between major cations (Ca^{2+}, Mg^{2+}, K^{+}, a) and a major anion (SO_4^{2-}), bromide (b) and chloride concentrations in the water column of Copano Bay. The solid lines are the dilution line of seawater. Note that seawater K^{+} and Ca^{2+} concentrations are very close, hence their dilution lines are indistinguishable from each other.

Table 4 Regression analysis between ions (Ca, Mg, K, sulfate, Br) and Cl in the water column of Copano Bay.

Regression	Slope	Intercept	R^2
Ca^{2+} vs. Cl^{-}	0.0190	0.2522	0.98
Mg^{2+} vs. Cl^{-}	0.0968	-0.6876	0.98
K^{+} vs. Cl^{-}	0.0179	0.9645	0.96
SO_4^{2-} vs. Cl^{-}	0.0508	0.6273	0.93
Br^{-} vs. Cl^{-}	0.0016	-0.0179	0.91

Pore Water Chemistry

Major ion chemistry

During both coring trips, i.e., prior to the August 2017 river discharge event and after the June 2018 discharge event, we observed lower Cl^- concentrations in the pore water than in the water column, although in 2017 sediment pore waters had higher Cl^- concentration than the 2018 ones along both the T2 and T4 transects (Figs. 9a and 10a). Along the T2 transect, $\delta^{13}C$ of pore water DIC did not appear to be significantly different between the two trips (Fig. 9b) although the 2018 values were less negative along the T4 transect than the T2. Regardless, pore water $\delta^{13}C$ values were all lower than the overlying water values. The lower pore water Cl^- concentration suggest that SGD discharge was likely occurring during both coring periods, regardless of the river discharge conditions. This is also consistent with the notion that SGD discharge plays a more important role in supplying freshwater to the semiarid coastal estuaries (Spalt et al., 2018).

Consistent with Cl^- difference between the two coring periods (i.e., lower in 2018 than in 2017), both $\delta^{18}O$ and δD showed higher values in 2017 (before the 2017 river discharge event) than in 2018 (after the 2018 discharge event), indicating that pore water in 2017 likely was likely derived from source water that experienced greater evaporation, hence the heavier isotopes were enriched, compared with that in 2018.

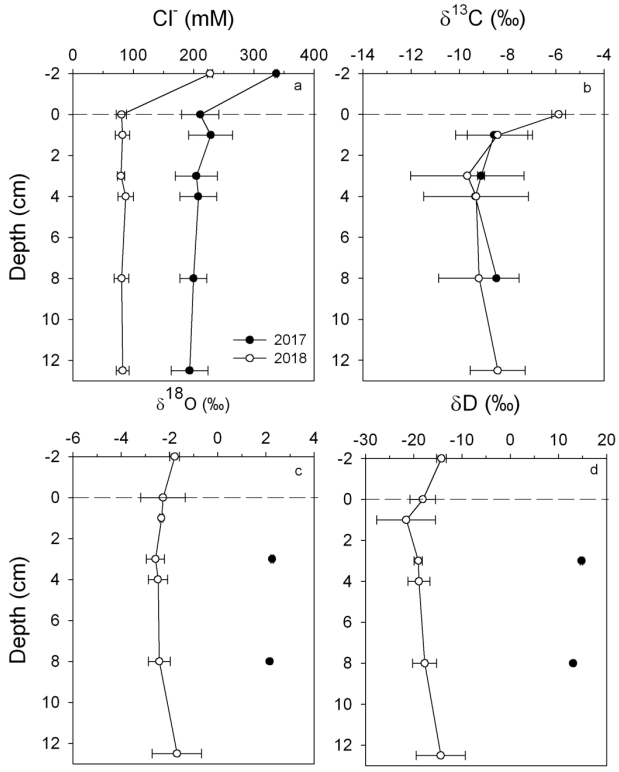

Figure 9 Pore water profiles of Cl^-, $\delta^{13}C$, $\delta^{18}O$, and δD along the T2 transect (Fig. 1). The dashed lines represent sediment-water interface. The bottom water values are noted at -2 cm.

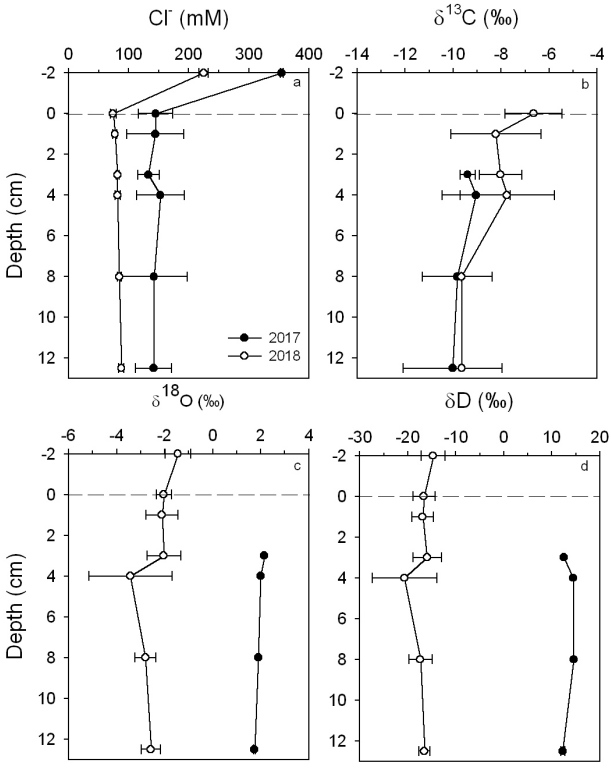

Figure 10 Pore water profiles of Cl^-, $\delta^{13}C$, $\delta^{18}O$, and δD along the T4 transect (Fig. 1). The dashed lines represent sediment-water interface. The bottom water values are noted at -2 cm.

Similar to Cl^- profiles, all major ions (except Br^- data that were not obtained due to sample preservation issue) showed higher concentration in 2017 than in 2018 (Figs. 11 and 12). The most conspicuous difference between the two sets of pore waters was that the core bottom appeared to have higher ion concentrations than shallower core and bottom water in 2018, while the 2017 profiles suggested either little downcore changes (K^+, Fig. 12c) in the ion concentrations or decreasing trends (all other ions). Therefore, considering the higher ionic concentrationss in 2017 (Figs. 9-12) and similar SGD rates (Table 2), SGD during the dry period (2017) must have supplied more ions to the water column than during the wet period (2018) (Table 2).

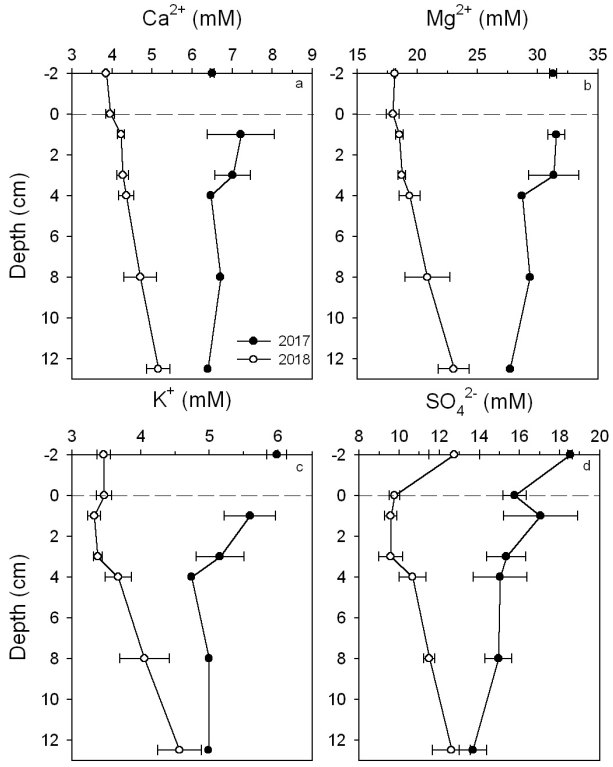

Figure 11 Pore water major ions profiles (Ca^{2+}, Mg^{2+}, K^{+}, SO_4^{2-}) along the T2 transect (Fig. 1). The dashed lines represent sediment-water interface. The bottom water values are noted at -2 cm.

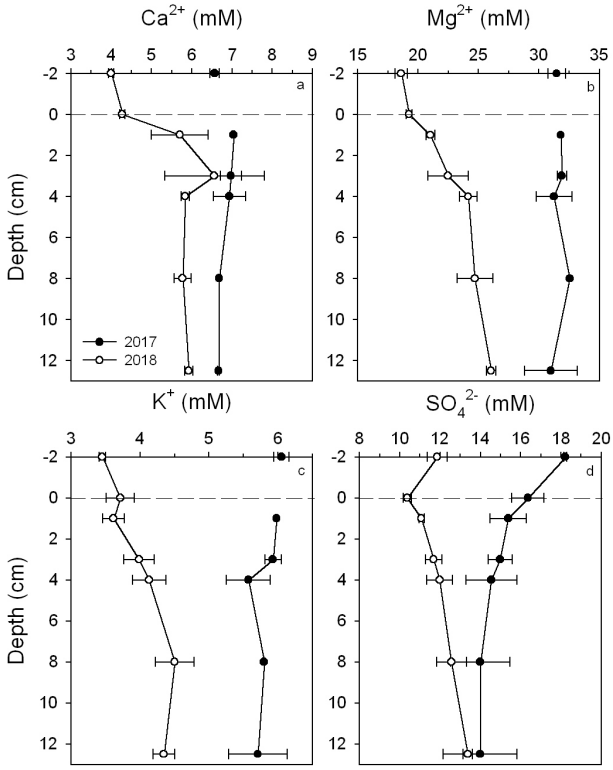

Figure 12 Pore water major ions profiles (Ca^{2+}, Mg^{2+}, K^{+}, SO_4^{2-}) along the T4 transect (Fig. 1). The dashed lines represent sediment-water interface. The bottom water values are noted at -2 cm.

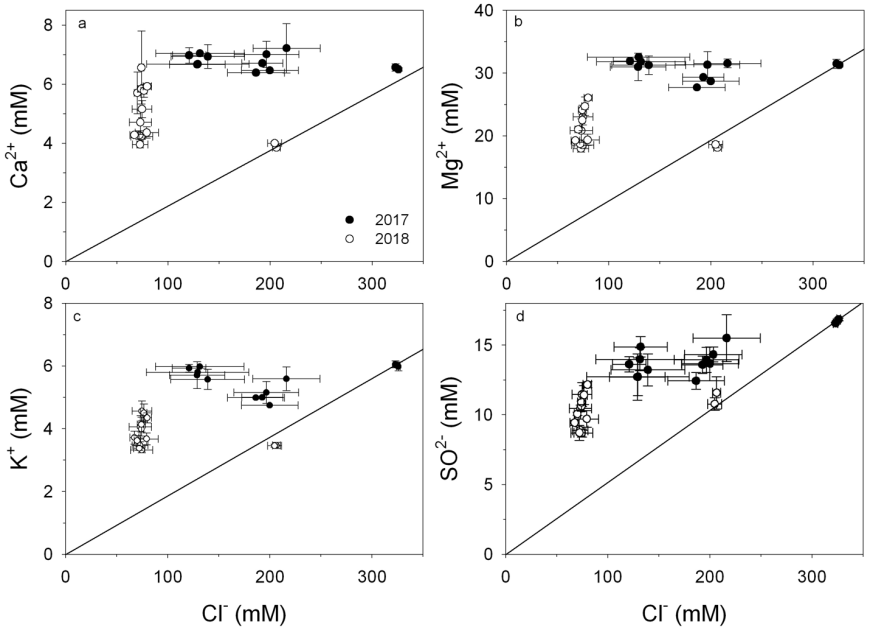

Figure 13 Correlations between major ions in pore water and water column during the time of core collection. The straight lines represent the seawater dilution line. The set of data falling on or near the straight lines were from the water column.

Unlike in the water column where all major ions exhibited excellent linear relationship with Cl^- (Fig. 8), all major ions in pore water showed significant deviation (i.e., enrichment) from the seawater dilution lines (Fig. 13), indicative of highly enriched ions relative to simple seawater dilution, even though SO_4^{2-} appeared to be consumed in the pore water in 2017 (Fig. 11d). Sulfide, on the other hand, was not detected in all samples, possibly due to the presence of abundant iron in these sediments (Davis, 2017) that prevents the buildup of free sulfide (Canfield, 1989). Nevertheless, all measured excessive ions relative to Cl^- suggested that SGD would supply these ions to the estuarine water when discharge occurs.

Inorganic carbon chemistry

As expected, sediment pore water had higher total alkalinity and total dissolved inorganic carbon than both the overlying water and the water column (Figs. 14 and 15), presumably as a result of anaerobic respiration.

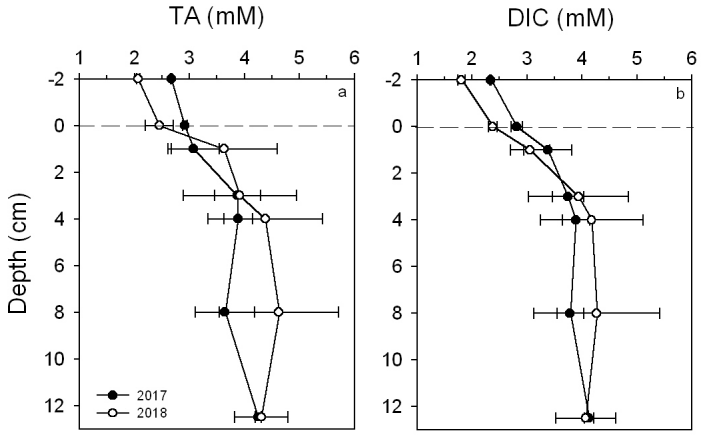

Figure 14 Total alkalinity (a) and total dissolved inorganic carbon (b) along the T2 transect (Fig. 1).

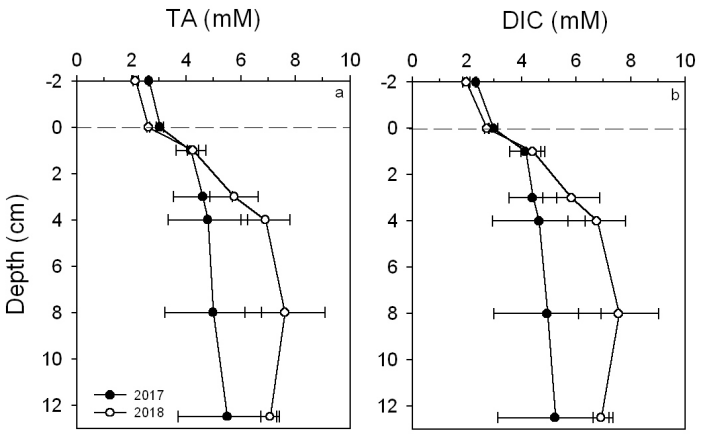

Figure 15 Total alkalinity (a) and total dissolved inorganic carbon (b) along the T4 transect (Fig. 1).

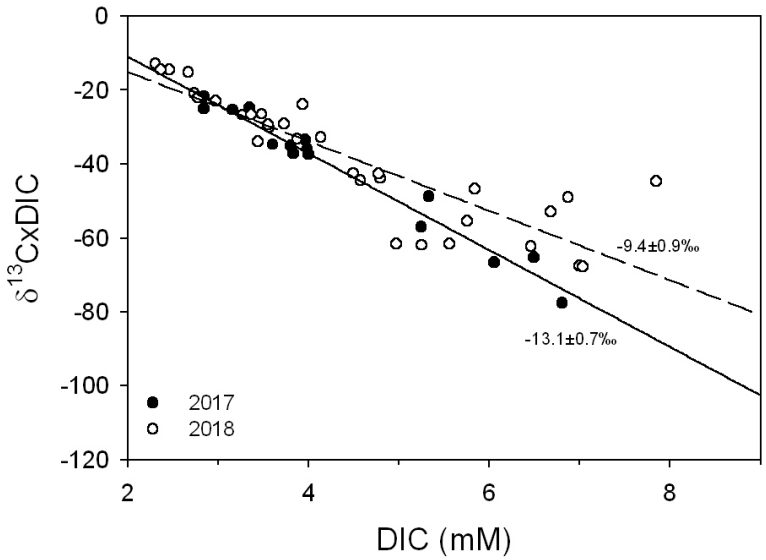

Figure 16 Stable carbon isotope of added CO_2 into sediment pore waters. The values are the regressed slopes from both 2017 (solid line) and 2018 (dashed line).

Using the approach in Hu and Burdige (2007), the $\delta^{13}C$ value of CO_2 added into the sediment pore water can be calculated using the regression between $\delta^{13}C$xDIC and DIC concentration. The 2017 data generated a value -13.1±0.7‰ ($r^2 = 0.97$) while the 2018 data were significantly more scattered with a slope of -9.4±0.9 ($r^2 = 0.77$), and the scattered data were mostly one station on the T4 transect. Excluding these data points (not shown) will significantly improve the regression (slope = -11.4±0.7‰ and $r^2 = 0.90$). Nevertheless, the $\delta^{13}C$ signal of added CO_2 appeared to be very close to organic carbon produced by C4 plants (saltmarsh),

seagrasses, and benthic algae (Lebreton et al., 2016), indicating that these organic materials may be remineralized in the nearshore sediments in our studied area.

Stable H and O isotopes

The stable isotopes of $\delta^{18}O$ and δD data range was relatively significant given that there is small variability between the surveyed environments. The min $\delta^{18}O$ and δD of -5.41‰ and -34.0 ‰ were measured in one of the river surface water samples and one of the porewaters in August 2018 (Figure 17). The max $\delta^{18}O$ and δD of 2.28‰ and 15.0 ‰ was measured in August, 2017 pore waters. Seasonal changes are significant given the analytical precision (Fig. 17). Although surface water samples for July 2017 were not measured for $\delta^{18}O$ and δD, the available porewater shows enrichment above the typical seawater signatures (Michener and Lajtha, 2007) and the August 2018 data. Enriched δD and $\delta^{18}O$ ratios are associated with lower amounts of rainfall and higher evaporation rates (Katz et al., 1997), conditions captured in July 2017 (Figure 6). The more enriched $\delta^{18}O$ and δD porewater signatures in July 2018 (1.67 and 10.67‰, respectively) reflect the effects of evaporation on the soils and infiltrating groundwater. In semi-arid coastal settings, meteoric groundwater discharge is not necessarily fresh due to high evaporation effects, as shown by the isotopically enriched $\delta^{18}O$ and δD signatures reported in shallow groundwater just south of Aransas Bay (Bighash and Murgulet, 2015; Murgulet et al., 2016). In average, deep porewater $\delta^{18}O$ and δD signatures (-1.63 and -12.55‰, respectively) closely match surface water (-1.14 and -8.93‰, respectively) in August 2018.

Similar seasonal shifts are observed in the porewater extracted from the shallow sediment profiles. A shift of approximately 4‰ and 20‰ for $\delta^{18}O$ and δD, respectively towards more negative signatures is observed based on four core data (Figures 9 and 10). As mentioned earlier in the ***Radium Activities and SGD Rates*** section, there is a shift in deep porewater signatures

towards more depleted ratios, an indication of lateral transport of shallow fresh groundwater within the subterranean estuary. The input of fresher groundwater to the estuary is, thus evidenced by the significant change in the isotope signature in the deeper and shallower pore water, also reflected by changes in salinity, radium, and major ion chemistry.

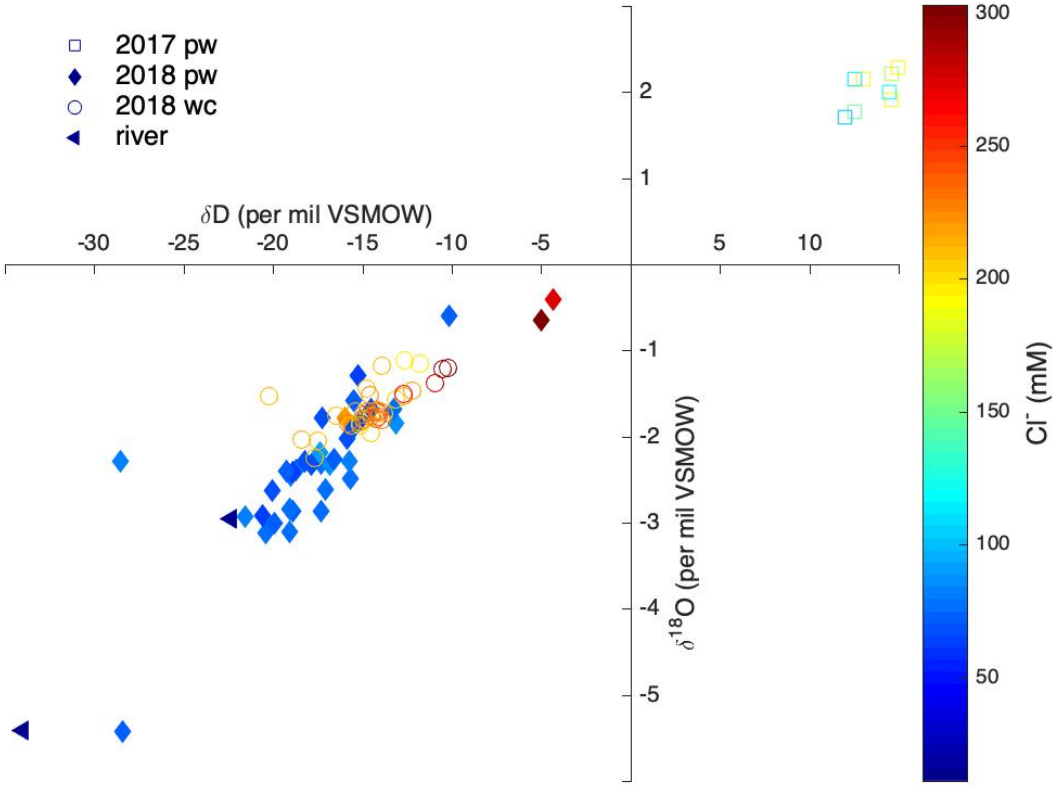

Figure 17 Stable H and O isotope compositions of pore water (square and diamond, pw), water column (circle, wc), and Mission River water (triangles, r).

Sediment Alkalinity and DIC Fluxes

Using deep pore water concentrations and the calculated SGD rates, apparent discharges of alkalinity and DIC were calculated (Fig. 18).

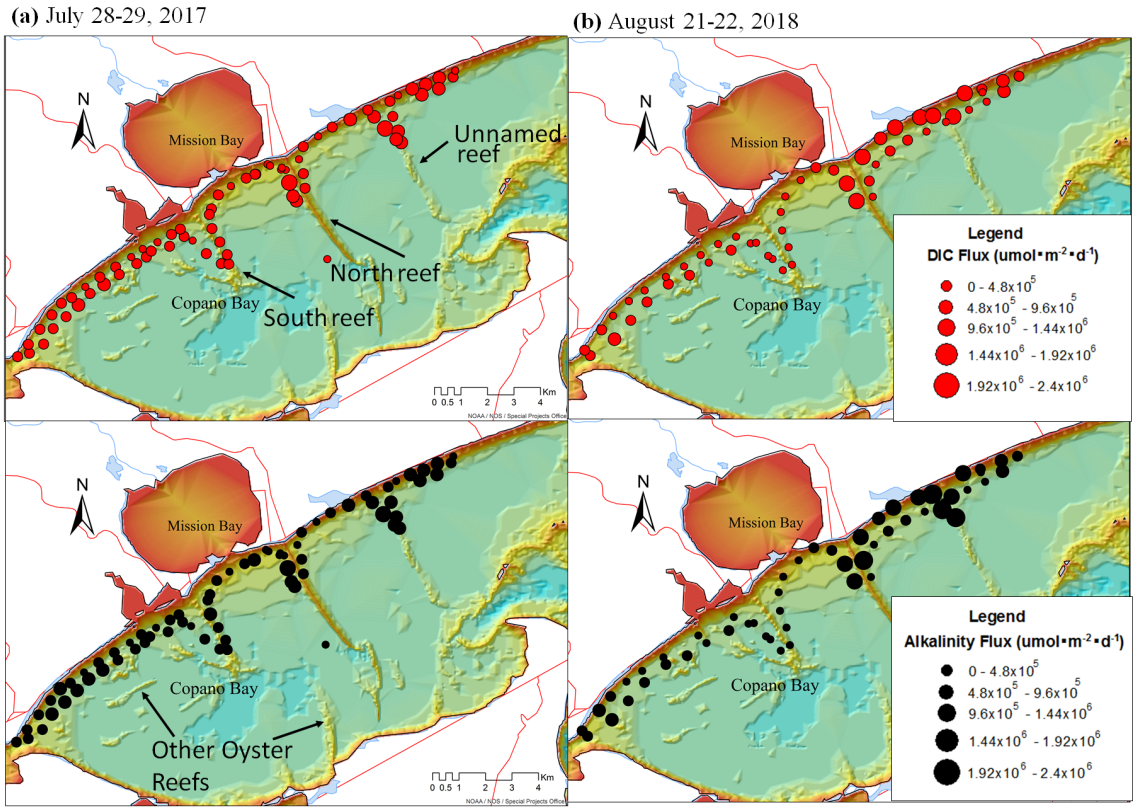

Figure 18 SGD induced benthic fluxes of alkalinity and DIC into bay water.

The calculated SGD-induced alkalinity and DIC fluxes in July 2017 were 0.20-1.55 and 0.22-1.62 mol m^{-2} d^{-1}, respectively, and the values in August 2018 were 0.03-2.36 and 0.03-2.37 mol m^{-2} d^{-1}, respectively. The average values were similar, i.e., 0.79±0.33 mol m^{-2} d^{-1} for alkalinity and 0.74±0.33 mol m^{-2} d^{-1} for DIC in July 2017, and 0.81±0.67 mol m^{-2} d^{-1} for alkalinity and 0.80±0.67 mol m^{-2} d^{-1} for DIC in August 2018. These values are similar to the fluxes calculated using the same method in Nueces Bay in 2014-2016, south of Copano Bay (Murgulet et al., 2018).

On the other hand, diffusive alkalinity and DIC flux based on Fick's first law (Berner, 1980) using the concentration gradient between the topmost porewater (0.5 cm) and the bottom water in July 2017 were 0-0.06 and 0.02-0.08 mol m^{-2} d^{-1}, respectively, and the values in August 2018 were 0.03-0.07 and 0.03-0.09 mol m^{-2} d^{-1}, respectively. The average values were 0.03±0.02 mol m^{-2} d^{-1} for alkalinity and 0.04±0.02 mol m^{-2} d^{-1} for DIC in July 2017 and 0.05±0.02 mol m^{-2} d^{-1} for alkalinity and 0.05±0.03 mol m^{-2} d^{-1} for DIC in August 2018.

Clearly, the two types of benthic flux estimations were different in both the values (SGD generated fluxes were an order of magnitude higher than the diffusive fluxes) and the relative extent of fluxes. Alkalinity flux was greater than DIC flux by ~5% using the SGD data. These results are primarily due to the fact that alkalinity concentrations were slightly higher than those for DIC in the deep groundwater. On the other hand, diffusive DIC flux was greater (by 28%) than alkalinity flux (paired t-test, $p<0.005$, $n=11$) if excluding a sediment core collected on August 16, 2018 (28.10471˚, -97.19263˚) as we suspect analytical error with the DIC sample (the concentration of alkalinity was 4.74 mM and that for DIC was 3.44 mM), and typical alkalinity and DIC in shallow porewaters seldom deviates from the 1:1 relationship, regardless of carbonate dissolution or sulfate reduction (Burdige, 2006).

The difference in calculated fluxes using the two approaches (i.e., an order of magnitude) is consistent with other groundwater studies (i.e., Liu et al., 2014). However, both the Liu et al. study and many other studies in marine sediment (see a summary in Hu and Cai, 2011) suggest higher DIC flux than that for alkalinity, due to oxidation of dissolved reduced species (reduced metals, ammonia, and sulfide) from the upwelled anoxic pore water or groundwater. Therefore, more studies are needed to quantify the net contribution of benthic flux (both SGD and diffusive flux) on the estuarine carbonate system.

SUMMARY

The goal of this study was to examine the role of SGD in exporting acidity to the semiarid Copano Bay, the southernmost coastal bay that sustains commercial oyster production. Our fieldwork covered two periods of drying up conditions (prior to August 2017 and between August 2017 and June 2018)) and a period of substantial precipitation and river discharge. The changing hydrological conditions apparently influenced the sediment pore water as well, as the 2018 data collected during a wet period revealed substantially more freshwater abundance compared to the 2017 data from the end of a dry period. Regardless of the hydrological condition, the pore water data suggest that SGD occurred under both dry and wet conditions.

While the water column ions showed nearly ubiquitous dilution of seawater, pore waters showed much elevated major ions (Mg^{2+}, Ca^{2+}, K^{+}, and SO_4^{2-}) relative to Cl^{-}, indicative of either production within the sediment or the ions being transported along with the SGD, which has substantially different composition than the estuarine water.

The excess ions, especially SO_4^{2-}, it if is being produced through the oxidation of reduced sulfur, not only could be a significant source of acidity to the Copano Bay, but other coastal bays in the semiarid south Texas.

SGD and diffusive fluxes of alkalinity and DIC differed by an order of magnitude with the SGD-derived rates being greater. The diffusive DIC flux is ~28% greater than that for alkalinity although the rates calculated using SGD had higher alkalinity flux (by ~5% overall). Further studies are needed to examine the extent of oxidation of reduced species from the upwelled groundwater to investigate the role of benthic contribution to the estuarine carbonate system.

REFERENCES CITED

Amara, l.V., Cabral, H.N. and Bishop, M.J., 2012. Effects of estuarine acidification on predator-prey interactions. Marine Ecology Progress Series, 445, 117-127.

Andersson, A.J. and Gledhill, D., 2013. Ocean acidification and coral reefs: effects on breakdown, dissolution, and net ecosystem calcification. Annual Review of Marine Science, 5, 321-348.

Berner, R.A., 1980. Early diagenesis - A Theoretical Approach. Princeton series in geochemistry. Princeton University Press, Princeton, N.J., 256 pp.

Beseres Pollack, J., Yoskowitz, D., Kim, H.-C. and Montagna, P.A., 2013. Role and value of nitrogen regulation provided by oysters *Crassostrea virginica* in the Mission-Aransas Estuary, Texas, USA. PLoS ONE, 8, e65314.

Bighash, P. and Murgulet, D., 2015. Application of factor analysis and electrical resistivity to understand groundwater contributions to coastal embayments in semi-arid and hypersaline coastal settings. Science of The Total Environment, 532, 688-701.

Brandes, J.A., 2009. Rapid and precise δ13C measurement of dissolved inorganic carbon in natural waters using liquid chromatography coupled to an isotope‐ratio mass spectrometer. Limnology and Oceanography: Methods, 7, 730-739.

Burdige, D.J., 2006. Geochemistry of Marine Sediments. Princeton University Press, 609 pp.

Burnett, W.C. and Dulaiova, H., 2003. Estimating the dynamics of groundwater input into the coastal zone via continuous radon-222 measurements. Journal of Environmental Radioactivity, 69, 21-35.

Burnett, W.C., Taniguchi, M. and Oberdorfer, J., 2001. Measurement and significance of the direct discharge of groundwater into the coastal zone. Journal of Sea Research, 46, 109-116.

Canfield, D.E., 1989. Reactive iron in marine sediments. Geochimica et Cosmochimica Acta, 53, 619-632.

Carter, B.R., Radich, J.A., Doyle, H.L. and Dickson, A.G., 2013. An automatic system for spectrophotometric seawater pH measurements. Limnology and Oceanography: Methods, 11, 16-27.

Cerdà-Domènech, M., Rodellas, V., Folch, A. and Garcia-Orellana, J., 2017. Constraining the temporal variations of Ra isotopes and Rn in the groundwater end-member: Implications for derived SGD estimates. Science of The Total Environment, 595, 849-857.

Charette, M.A., Buesseler, K.O. and Andrews, J.E., 2001a. Utility of radium isotopes for evaluating the input and transport of groundwater-derived nitrogen to a Cape Cod estuary. Limnology and Oceanography, 46, 465-470.

Charette, M.A., Buesseler, K.O. and Andrews, J.E., 2001b. Utility of radium isotopes for evaluating the input and transport of groundwater‐derived nitrogen to a Cape Cod estuary. Limnology and Oceanography, 46, 465-470.

Corbett, D.R., Burnett, W.C., Cable, P.H. and Clark, S.B., 1998. A multiple approach to the determination of radon fluxes from sediments. Journal of Radioanalytical and Nuclear Chemistry, 236, 247-252.

Davis, R.A., 2017. Sediments of the Gulf of Mexico. In: C.H. Ward (Editor), Habitats and Biota of the Gulf of Mexico: Before the Deepwater Horizon Oil Spill: Volume 1: Water Quality, Sediments, Sediment Contaminants, Oil and Gas Seeps, Coastal Habitats,

Offshore Plankton and Benthos, and Shellfish. Springer New York, New York, NY, pp. 165-215.
de Weys, J., Santos, I.R. and Eyre, B.D., 2011. Linking groundwater discharge to severe estuarine acidification during a flood in a modified wetland. Environmental Science & Technology, 45, 3310-3316.
Dickson, A.G., Afghan, J.D. and Anderson, G.C., 2003. Reference materials for oceanic CO_2 analysis: a method for the certification of total alkalinity. Marine Chemistry, 80, 185-197.
Dimova, N., Burnett, W.C., Horwitz, E.P. and Lane-Smith, D., 2007. Automated measurement of Ra-224 and Ra-226 in water. Applied Radiation and Isotopes, 65, 428-434.
Dimova, N.T., Burnett, W.C. and Speer, K., 2011. A natural tracer investigation of the hydrological regime of Spring Creek Springs, the largest submarine spring system in Florida. Continental Shelf Research, 31, 731-738.
Douglas, A.R., Murgulet, D. and Perterson, R., in review. Spatial and temporal variability of submarine groundwater discharge to a disturbed semi-arid estuary.
Dulaiova, H., Burnett, W.C., Chanton, J.P., Moore, W.S., Bokuniewicz, H.J., Charette, M.A. and Sholkovitz, E., 2006. Assessment of groundwater discharges into West Neck Bay, New York, via natural tracers. Continental Shelf Research, 26, 1971-1983.
Durridge, 2015. RAD7 Radon Detector User Manual, Billerica, MA, USA.
Elsinger, R.J. and Moore, W.S., 1980. 226Ra behavior in the pee Dee River-Winyah Bay estuary. Earth and Planetary Science Letters, 48, 239-249.
Feely, R.A., Sabine, C.L., Lee, K., Berelson, W., Kleypas, J., Fabry, V.J. and Millero, F.J., 2004. Impact of anthropogenic CO_2 on the $CaCO_3$ system in the oceans. Science, 305, 362-366.
Gardner, W.S., McCarthy, M.J., Carini, S.A., Souza, A.C., Lijun, H., McNeal, K.S., Puckett, M.K. and Pennington, J., 2009. Collection of intact sediment cores with overlying water to study nitrogen- and oxygen-dynamics in regions with seasonal hypoxia. Continental Shelf Research, 29, 2207-2213.
Hagens, M., Hunter, K.A., Liss, P.S. and Middelburg, J.J., 2014. Biogeochemical context impacts seawater pH changes resulting from atmospheric sulfur and nitrogen deposition. Geophysical Research Letters, 41, 2013GL058796.
Hassellöv, I.-M., Turner, D.R., Lauer, A. and Corbett, J.J., 2013. Shipping contributes to ocean acidification. Geophysical Research Letters, 40, 2731-2736.
Hu, X., Beseres Pollack, J., McCutcheon, M.R., Montagna, P.A. and Ouyang, Z., 2015. Long-term alkalinity decrease and acidification of estuaries in Northwestern Gulf of Mexico. Environmental Science & Technology, 49, 3401–3409.
Hu, X. and Burdige, D.J., 2007. Enriched stable carbon isotopes in the pore waters of carbonate sediments dominated by seagrasses: evidence for coupled carbonate dissolution and reprecipitation. Geochimica et Cosmochimica Acta, 71, 129-144.
Hu, X. and Cai, W.-J., 2011. The impact of denitrification on the atmospheric CO_2 uptake potential of seawater. Marine Chemistry, 127, 192-198.
Hu, X. and Cai, W.-J., 2013. Estuarine acidification and minimum buffer zone—A conceptual study. Geophysical Research Letters, 40, 5176-5181.
Jeffrey, L.C., Maher, D.T., Santos, I.R., McMahon, A. and Tait, D.R., 2016. Groundwater, acid and carbon dioxide dynamics along a coastal wetland, lake and estuary continuum. Estuaries and Coasts, 1-20.

Katz, B.G., Coplen, T.B., Bullen, T.D. and Davis, J.H., 1997. Use of chemical and isotopic tracers to characterize the interactions between ground water and surface water in mantled karst. Groundwater, 35, 1014-1028.

Kim, G., Burnett, W.C., Dulaiova, H., Swarzenski, P.W. and Moore, W.S., 2001. Measurement of Ra-224 and Ra-226 activities in natural waters using a radon-in-air monitor. Environmental Science & Technology, 35, 4680-4683.

Kleypas, J.A. and Yates, K.K., 2009. Coral reefs and ocean acidification. Oceanography, 22, 109-117.

Knee, K.L., Garcia-Solsona, E., Garcia-Orellana, J., Boehm, A.B. and Paytan, A., 2011. Using radium isotopes to characterize water ages and coastal mixing rates: A sensitivity analysis. Limnology and Oceanography-Methods, 9, 380-395.

Lebreton, B., Beseres Pollack, J., Blomberg, B., Palmer, T.A., Adams, L., Guillou, G. and Montagna, P.A., 2016. Origin, composition and quality of suspended particulate organic matter in relation to freshwater inflow in a South Texas estuary. Estuarine, Coastal and Shelf Science, 170, 70-82.

Lee, J.-M. and Kim, G., 2006. A simple and rapid method for analyzing radon in coastal and ground waters using a radon-in-air monitor. Journal of Environmental Radioactivity, 89, 219-228.

Lin, C., Wood, M., Haskins, P., Ryffel, T. and Lin, J., 2004. Controls on water acidification and de-oxygenation in an estuarine waterway, eastern Australia. Estuarine Coastal and Shelf Science, 61, 55-63.

Liu, Q., Charette, M.A., Henderson, P.B., McCorkle, D.C., Martin, W. and Dai, M., 2014. Effect of submarine groundwater discharge on the coastal ocean inorganic carbon cycle. Limnology and Oceanography, 59, 1529-1554.

Lopez, C., Murgulet, D. and Douglas, A., 2018. Impacts of Temporal and Spatial Variation of Submarine Groundwater Discharge on Nutrient Fluxes to Texas Coastal Embayments, Phase III (Baffin Bay). Scientific report submitted to Texas General Land Office, April 2018. GLO Contract No. 16-060-000-9104. p 105.

Michener, R.H. and Lajtha, K. (Editors), 2007. Stable Isotopes in Ecology and Environmental Science. Blackwell Publishing, 566 pp.

Montagna, P., Palmer, T.A. and Beseres Pollack, J., 2013. Hydrological Changes and Estuarine Dynamics. Springer Briefs in Environmental Sciences, 8. Springer, New York.

Montagna, P., Vaughan, B. and Ward, G., 2011. The importance of freshwater inflows to Texas estuaries. In: R.C. Griffin (Editor), Water Policy in Texas: Responding to the Rise of Scarcity. The RFF Press, Washington D.C., pp. 107-127.

Moore, W.S., 1996. Large groundwater inputs to coastal waters revealed by Ra-226 enrichments. Nature, 380, 612-614.

Moore, W.S., 2006. Radium isotopes as tracers of submarine groundwater discharge in Sicily. Continental Shelf Research, 26, 852-861.

Murgulet, D., Murgulet, V., Spalt, N., Douglas, A. and Hay, R.G., 2016. Impact of hydrological alterations on river-groundwater exchange and water quality in a semi-arid area: Nueces River, Texas. Science of The Total Environment, 572, 595-607.

Murgulet, D., Trevino, M., Douglas, A., Spalt, N., Hu, X. and Murgulet, V., 2018. Temporal and spatial fluctuations of groundwater-derived alkalinity fluxes to a semiarid coastal embayment. Science of The Total Environment, 630, 1343-1359.

NOAA, 2016. Annual Climatological Summary 1995-2015, WELDER W LIFE FOUND. In: N.O.a.A.A.N.C.D. Center (Editor).
NOAA (National Oceanic and Atmospheric Administration), 2014. National Weather Service.
Ruiz-Halpern, S., Maher, D.T., Santos, I.R. and Eyre, B.D., 2015. High CO2 evasion during floods in an Australian subtropical estuary downstream from a modified acidic floodplain wetland. Limnology and Oceanography, 60, 42-56.
Sammut, J., Melville, M.D., Callinan, R.B. and Fraser, G.C., 1995. Estuarine acidification: Impacts on aquatic biota of draining acid sulphate soils. Australian Geographical Studies, 33, 89-100.
Sammut, J., White, I. and Melville, M., 1996. Acidification of an estuarine tributary in eastern Australia due to drainage of acid sulfate soils. Marine and Freshwater Research, 47, 669-684.
Santos, I.R., Cook, P.L., Rogers, L., Weys, J.d. and Eyre, B.D., 2012. The "salt wedge pump": Convection-driven pore-water exchange as a source of dissolved organic and inorganic carbon and nitrogen to an estuary. Limnology and Oceanography, 57, 1415-1426.
Spalding, C., Finnegan, S. and Fischer, W.W., 2017. Energetic costs of calcification under ocean acidification. Global Biogeochemical Cycles, 31, 866-877.
Spalt, N., Murgulet, D. and Hu, X., 2018. Relating estuarine geology to groundwater discharge at an oyster reef in Copano Bay, TX. Journal of Hydrology, 564, 785-801.
Sun, Y. and Torgersen, T., 1998. The effects of water content and Mn-fiber surface conditions on Ra-224 measurement by Rn-220 emanation. Marine Chemistry, 62, 299-306.
Swarzenski, P.W., 2007. U/Th Series Radionuclides as Coastal Groundwater Tracers. Chemical Reviews, 107, 663-674.
Waldbusser, G.G., Hales, B., Langdon, C.J., Haley, B.A., Schrader, P., Brunner, E.L., Gray, M.W., Miller, C.A. and Gimenez, I., 2014. Saturation-state sensitivity of marine bivalve larvae to ocean acidification. Nature Climate Change, 5, 273-280.
Waldbusser, G.G. and Salisbury, J.E., 2014. Ocean acidification in the coastal zone from an organism's perspective: multiple system parameters, frequency domains, and habitats. Annual Review of Marine Science, 6, 221-247.
Webster, I.T., Hancock, G.J. and Murray, A.S., 1995. Modelling the effect of salinity on radium desorption from sediments. Geochimica et Cosmochimica Acta, 59, 2469-2476.
Williams, R.G. and Follows, M.J., 2011. Ocean dynamics and the carbon cycle: Principles and mechanisms. Cambridge University Press.
Yao, H. and Hu, X., 2017. Responses of carbonate system and CO2 flux to extended drought and intense flooding in a semiarid subtropical estuary Limnology & Oceanography, 62, S112-S130.